# The Impact of aerosol–ice nuclei-cloud interactions on a Typical Spring Dust-Precipitation Event in China

Jian Zhang[1,2], Chunhong Zhou[2]*, Xiaoyu Shen[2,3], Hong Wang[2,4], Sunling Gong[2,4,5,6], Xiaoye Zhang[2,4]

[1] Key Laboratory for Aerosol-Cloud-Precipitation of China Meteorological Administration, Nanjing University of Information Science & Technology, Nanjing, Jiangsu, China

[2] Institute of Atmospheric Composition and Environmental Meteorology & Key Laboratory of Atmospheric Chemistry of CMA, Chinese Academy of Meteorological Sciences, Beijing, China

[3] Key Laboratory of Urban Air Particulate Pollution Prevention and Control of Ministry of Ecology and Environment, College of Environmental Science and Engineering, Nankai University, Tianjin, China

[4] State Key Laboratory of Severe Weather, Chinese Academy of Meteorological Sciences, Beijing, China

[5] National Observation and Research Station of Coastal Ecological Environments in Macao, Macao Environmental Research Institute, Macau University of Science and Technology, Macao, China

[6] Research Institute for Pollution and Carbon Mitigation Assessment, Tianfu Yongxing Laboratory, Sichuan Chengdu, China

* Corresponding authors.

E-mail addresses: zhouch@cma.gov.cn (Chunhong Zhou)

带格式的: 英语(英国)

**Abstract**.

To investigate the impact of ice nuclei (IN) activated by dust aerosols on precipitation over China, this study uses regional Global/Regional Assimilation and Prediction System – China Meteorological Administration Unified Atmospheric Chemistry Environment (GRAPES/CUACE). The original temperature-dependent IN nucleation scheme in the Double-Moment 6-Class (WDM6) is improved by incorporating an on-line aerosol–IN nucleation scheme to examine their effects during a typical dust affected precipitation event in East Asia.

Dust modifies the spatial distribution and number concentration of IN, affecting heterogeneous ice nucleation. Compared with the systematic underestimation in original WDM6, the peak values of nucleated INs reach $10^{-4}$ $L^{-1}$ with the improved scheme, which is closer to observations.

Dust inhibit the development of clouds. Above 7 km, dust suppresses both heterogeneous nucleation and deposition growth. Thus, the total production rate of cloud ice drops to less than 24% of that in the control test T_CTL, promoting snow

formation and reducing the total ice-phase hydrometeor content to 70–85% of T_CTL. Between 4 and 7 km, dust enhances heterogeneous nucleation of cloud ice but suppresses deposition growth, leading to a decrease in the total ice-phase hydrometeor content to 85–91% of T_CTL. Below 4 km, dust suppresses the conversion of water vapor to cloud water, thereby reducing the liquid-phase hydrometeor content to 90–95% of T_CTL.

Dust modifies the precipitation distribution, bringing it closer to observations. It suppresses precipitation near dust source areas, where mean precipitation decreased by about 4.5 mm, while the downstream event-mean precipitation increased by about 1.1 mm.

Keywords: aerosol–IN–cloud–precipitation interactions；dust-precipitation event；on-line aerosol–IN nucleation scheme, CUACE

## 1 Introduction

The formation of cloud ice is one of the key processes in ice-phase precipitation, and ice nuclei (IN) associated with aerosols play a crucial role in the development of cloud ice, particularly in mid- to high-latitude areas and in the upper troposphere (Li et al., 2022; Chen et al., 2023; Knopf and Alpert, 2023). This is because homogeneous nucleation without IN occurs only below −40 °C, which is relatively rare in natural atmospheric environments (Eastwood et al., 2008; Herbert et al., 2015; Kumar et al., 2020; Che et al., 2021). In contrast, heterogeneous nucleation mediated by IN can occur under ice-supersaturated conditions at much higher temperatures, making it the dominant pathway for cloud ice formation.

Aerosols can serve as IN, participating in cloud formation, altering cloud microphysical properties and lifetimes, and thereby affecting precipitation (Albrecht, 1989; Andreae and Crutzen, 1997). Among different species, mineral dust is recognized as one of the primary sources of atmospheric IN (Khain et al., 2000; Nenes et al., 2014; Tobo et al., 2019). Dust particles have unique surface structures that facilitate the adsorption and binding of water molecules, promoting the formation of cloud ice (Possner et al., 2017; Stevens et al., 2018). Stith et al. (2009) and DeMott et al. (2015) have found a strong correlation between IN number concentration and aerosols with diameters larger than 0.5 μm, with mineral dust accounting for 33-50% of the total IN. Jiang et al. (2016) combined IN measurements during dust conditions at multiple sites in China, including Xinjiang (Jiang et al., 2016), Mt. Huangshan(Jiang et al., 2015), and Nanjing (Yang et al., 2013), and found that IN concentrations were significantly higher than those under non-dust conditions. ~~Jiang et al. (2016) observed that IN concentrations observed during dust events in Huangshan, Xinjiang and Nanjing were significantly higher than those under non-dust conditions.~~ Tobo et al. (2020) observed that IN concentrations increased remarkably during dust events in Tokyo when temperatures were above −25 °C. In addition, aged dust aerosol has increased solubility, which can act as cloud condensation nuclei (CCN) and thereby further influencing precipitation (Trochkine et al., 2003).

Compared with the relatively well-understood impacts of aerosols as CCN, the

域代码已更改
域代码已更改
域代码已更改
域代码已更改
域代码已更改
域代码已更改
带格式的: 字体: (中文) 宋体, 字体颜色: 黑色, 非突出显示
域代码已更改
带格式的
带格式的: 字体: (中文) 宋体, 字体颜色: 黑色, 非突出显示
域代码已更改
带格式的
带格式的: 字体: (中文) 宋体, 字体颜色: 黑色, 非突出显示
带格式的
带格式的: 字体: (中文) 宋体, 字体颜色: 黑色, 非突出显示
域代码已更改
域代码已更改
域代码已更改
域代码已更改
带格式的: 字体: 10.5 磅

role of dust as IN is considerably more complex and remains poorly understood, with substantial uncertainties (Kaufman et al., 2002; Eastwood et al., 2008; Pan et al., 2017; Possner et al., 2017). ~~Observational studies have reported diverse and sometimes contradictory relationships between dust and precipitation, depending on temporal scale, season, and environmental conditions.~~ Based on chemistry (WRF-Chem) model and multiple observational and reanalysis data, Wang et al. (2024) found that dust aerosols can suppress light precipitation by increasing atmospheric stability and inhibiting the conversion of cloud droplets into raindrops. ~~Temporal scale and seasonality play a critical role in shaping the observed relationships between dust and precipitation. At interannual scales, Han et al. (2008) found a significant negative correlation between dust storm frequency and precipitation over the Taklimakan Desert, whereas a positive correlation was observed at monthly scales, suggesting that dust precipitation relationships are scale dependent. Seasonal contrasts have also been reported. Using long-term ground-based observations, Wang (2013) showed that dust aerosols tend to suppress precipitation over arid and semi-arid regions in spring but may enhance precipitation in summer. In addition to temporal variability, the impacts of dust on clouds and precipitation also exhibit strong regional and environmental dependence.~~ In contrast, Naeger (2018) found that dust could enhance precipitation over Florida based on multi-sensor satellite observations and field campaigns. More recently, Hu et al. (2023) demonstrated that the impact of springtime dust on precipitation is strongly modulated by the presence of other aerosol types. Liu et al. (2024) analyzed the spatiotemporal patterns and trends of dust aerosols and precipitation and found that dust increases suppress precipitation over source regions such as the Gobi and Taklamakan deserts, but enhance precipitation in downwind areas like northern China. Overall, due to the multiple factors influencing precipitation beyond aerosols, it remains challenging to quantify the impact of dust on precipitation from observations alone (Zhou et al., 2016; Stier et al., 2024), highlighting the need for process-oriented numerical modeling studies with physically based aerosol–ice nucleation parameterizations.

Numerical model is a crucial approach for numerically studying the impact of dust

域代码已更改

域代码已更改

域代码已更改

域代码已更改

域代码已更改

域代码已更改

带格式的: 字体: (中文) 宋体, 12 磅, 字体颜色: 自动设置

带格式的: 字体: (中文) 宋体, 12 磅, 字体颜色: 自动设置

on precipitation. In early cloud microphysics scheme, the ice nucleation scheme did not account for aerosols, with IN concentrations typically expressed as functions of temperature or supersaturation (DeMott et al., 2010). Moreover, many clouds ice microphysical schemes were single-moment, which only simulated the mass mixing ratio of cloud ice. Such single-moment schemes often led to large biases in cloud ice mass concentrations (Molthan and Colle, 2012; Igel et al., 2015). In contrast, double-moment ice schemes, which simulate both cloud ice mass and number concentrations, outperform the single-moment schemes in terms of the simulated structure, life cycle, cloud coverage, precipitation, and microphysical properties (Pu and Lin, 2015; Zhao et al., 2021). The double-moment ice schemes can provide more stable and improved precipitation simulations (Kang et al., 2018; Shen et al., 2022; Shen et al., 2024). Mascioli et al. (2021) used the Thompson aerosol-aware microphysics scheme, incorporating the IN nucleation scheme of DeMott et al. (2010), to study the sensitivity of precipitation to different prescribed dust aerosol concentrations. Park and Lim (2023) develops the revised Weather Research and Forecasting Double-Moment 6-class (WDM6) scheme through the implementation of prognostic cloud ice number concentrations. The excess generation of cloud ice mixing ratio is considerably alleviated. However, these studies did not establish an explicit quantitative relationship between on-line aerosols and IN. Su and Fung (2018a) implemented the simplified Goddard Chemistry Aerosol Radiation and Transport aerosol model (GOCART) together with Shao's dust emission scheme (Kang et al., 2011; Shao et al., 2011) in WRF/Chem and incorporated the online IN nucleation scheme of DeMott et al. (2015) for producing real time IN into the double-moment Thompson–Eidhammer microphysics scheme. They analyzed the impact of dust on radiative forcing and temperature in East Asia, but only the sensitive impacts in terms of precipitation rate in March and April in 2012 (Su and Fung, 2018b). The spring of 2012 is not a typical dust season, most dust storm concentrated in Mongolia. Therefore, the microphysical pathways through which dust affects precipitation during typical dust events remain insufficiently studied. In this study, we focus on a representative spring dust–

域代码已更改
域代码已更改
域代码已更改
域代码已更改
域代码已更改
域代码已更改
域代码已更改
域代码已更改
域代码已更改

precipitation event and explicitly examine the cloud microphysical processes associated with dust-induced heterogeneous ice nucleation, together with direct comparisons to precipitation observations in the Global/Regional Assimilation and PrEdiction System, China Meteorological Administration (CMA) Unified Atmospheric Chemistry Environment (GRAPES/CUACE) model. GRAPES/CUACE provides on-line sectional aerosol concentrations with multi chemical composition information (Wang et al., 2010; Zhou et al., 2012). Zhou et al. (2016) introduced an on-line aerosol–CCN–cloud interaction scheme into the system, allowing the model to simulate real time CCN activation and their influence on precipitation. However, in the GRAPES/CUACE microphysics scheme WDM6, IN is a function of temperature only, and cloud ice is represented by a single-moment scheme only for the mass mixing ratio (Hong et al., 2004; Zhang et al., 2022). To address these limitations, this study implements a double-moment cloud ice scheme and incorporates an on-line aerosol–IN nucleation scheme to explicitly represent heterogeneous processes. Using this improved framework, we then investigate the impact of dust on precipitation by a typical dust affected precipitation event in East Asia. This paper is organized as follows: Section 2 introduces the model configuration, cloud microphysical processes, on-line aerosol–IN nucleation scheme, study region, and observational datasets. Section 3 presents the evaluation of the improved model's simulation performance and discusses the effects of dust on precipitation. Section 4 summarizes the main conclusions of the study.

域代码已更改

域代码已更改

域代码已更改

## 2 Model description and methodology

### 2.1 GRAPES/CUACE

The GRAPES is a fully compressible, non-hydrostatic numerical weather model that adopts a semi-implicit and semi-Lagrangian discretization scheme (Chen et al., 2008; Xu et al., 2008; Zhang and Shen, 2008; Wang et al., 2022a). The physical packages include cumulus convective, single-moment cloud microphysics, radiative, land surface, and boundary layer processes. CUACE is a regional chemical weather forecasting system developed by Gong and Zhang (2008) coupled on-line with GRAPES (Wang et al., 2010). It is capable of simulating on-line seven aerosol species

域代码已更改

域代码已更改

域代码已更改

of sulfate, nitrate, ammonium, black carbon, organic carbon, sea-salt together with dust (Zhou et al., 2008, 2012; Wang et al., 2015). The sectional dust emission scheme is by Marticorena and Bergametti (1995) and Alfaro and Gomes (2001) which has been improved by surface dust flux observations and desertification in East Asia (Gong et al., 2003), and new desertification map and soil texture samples from Chinese deserts (Zhou et al., 2019; Zhou et al., 2024). The aerosol size spectra have been divided into 12 size bins with a radius range of 0.005–0.01, 0.01–0.02, 0.02–0.04, 0.04–0.08, 0.08–0.16, 0.16–0.32, 0.32–0.64, 0.64–1.28, 1.28–2.56, 2.56–5.12, 5.12–10.24, and 10.24–20.48 μm. GRAPES/CUACE has a horizontal resolution of 0.15° and 31 vertical levels extending to approximately 28.6 km in altitude.

域代码已更改

域代码已更改

### 2.2 WDM6 microphysics scheme

In this study, we select the WDM6 microphysics scheme in GRAPES for simulating precipitation (Hong et al., 2004; Zhang et al., 2022) . The WDM6 scheme simulates the mass mixing ratio of water vapor (Qv), as well as the mass and number concentrations of cloud water (Qc) and rainwater (Qr) in warm clouds. For icy clouds, it includes the mass mixing ratios of cloud ice (Qi), snow (Qs), and graupel (Qg). A double-moment cloud ice scheme by Park and Lim (2023) is incorporated into the WDM6 scheme, allowing for the explicit prediction of cloud ice number concentration. A sectional CCN activated scheme has been introduced in WDM6 in GRAPES/CUACE, connecting the multi-component multi-section aerosols from CUACE into the WDM6 microphysics and the sub-grid convective parameterization scheme by newly activated CCN at each time step (Zhou et al., 2016).

域代码已更改

域代码已更改

### 2.3 On-line aerosol-IN nucleation scheme

In the original WDM6 scheme, when the temperature is below 0 ℃, the increase in cloud ice mass concentration arises from two processes: heterogeneous nucleation (Pigen) and deposition–sublimation of cloud ice (Pidep, when positive).~~In the original WDM6 scheme, when the temperature is below 0 ℃, the production rate of cloud ice is attributed to two processes: heterogeneous nucleation (Pigen) and deposition-sublimation rate of cloud ice (Pidep).~~ Both consume water vapor to form ice clouds.

The abbreviations for the remaining cloud microphysical processes are listed in Table 2. The IN concentration~~,~~ Nice ($m^{-3}$), is calculated by a classical ice nuclei nucleation scheme, which is an empirical function of temperature and does not account for the influence of atmospheric aerosols (Hong et al., 2004):

$$Nice\ \ N_{ice}(m^{-3}) = 10^3 e^{0.1(T_0 - T_k)} \quad (1)$$

Where，$T_k$ is atmospheric temperature，$T_0$ is the freezing point (273.15 K)。

This study implements an on-line aerosol-IN nucleation scheme in GRAPES/CUACE that accounts for heterogeneous ice nucleation processes influenced by atmospheric aerosols. Heterogeneous nucleation mechanisms are generally classified into immersion freezing, condensation freezing, deposition nucleation, and contact freezing (Hiranuma et al., 2015; Ilotoviz et al., 2016; Lee et al., 2017). Among these mechanisms, immersion freezing, condensation freezing, and deposition nucleation are selected, as they are relatively well developed. This selection is based on the fact that dust aerosols primarily affect ice nucleation at temperatures below 258.15 K through these three mechanisms (Cantrell et al., 2013; Patnaude et al., 2025), whereas the efficiency of contact freezing by dust particles is relatively low (Niehaus et al., 2014).

Immersion freezing is a heterogeneous ice nucleation process with existence of liquid drops at temperatures between 233.15 K and 273.15 K, which ice nucleus immersed in supercooled liquid, triggering it freezing into an ice crystal (Boose et al., 2016). Immersion freezing consumes water vapor to form cloud ice. The initial size of the ice crystal is influenced by the size of the liquid droplet (Fan et al., 2014; Gibbons et al., 2018), therefore the cloud ice formation through this mechanism is relatively easier compared to other nucleation mechanisms. The selected immersion freezing nucleation scheme here is developed by DeMott et al. (2015), based on continuous flow diffusion chamber measurements. The number concentration of ice nuclei, ~~$N_{icenui}$~~ Nicenui ($m^{-3}$), activated via immersion freezing is given by:

$$N_{icenui}\text{Nicenui}(m^{-3}) = 3 * n_{aer,0.5}^{1.25} * e^{(0.46*(273.16 - T_k) - 11.6)} \quad (2)$$

Where, $n_{aer,0.5}^{1.25}$ is the number concentration of insoluble aerosol particles with

域代码已更改
带格式的: 非突出显示
带格式的: 非突出显示
域代码已更改
域代码已更改
域代码已更改
域代码已更改
域代码已更改
域代码已更改
带格式的: 上标

diameters exceeding 0.5 μm such as dust, black carbon and part of organic carbon.

Deposition and condensation freezing are both heterogeneous ice nucleation processes that occur at temperatures between 248.15 K and 258.15 K (Chen et al., 2019). In condensation freezing, water vapor first condenses on the surface of IN and subsequently freezes to form an ice crystal, while in deposition nucleation, water vapor directly deposits onto the IN surface (Kanji et al., 2017). The ~~initial size of the ice crystals is comparable to that of the smallest droplets (Chen et al., 2019), and~~ the ice formation through these two pathways is generally harder than that through immersion freezing (DeMott et al., 2015). The parameterization used here follows the formulation of Chen et al. (2019). In Jiang et al. (2016), the ice-nucleating ability of dust aerosols was derived from measurements conducted at several sites in China (Yang et al., 2013; Jiang et al., 2015; Jiang et al., 2016), using a static vacuum vapor diffusion chamber based on the FRIDGE (Frankfurt Ice Nuclei Deposition Freezing Experiment) design. (Chen et al., (2019)further refined the parameterization to explicitly represent deposition and condensation freezing processes within a specified temperature range. ~~Chen et al. (2019) further refined the parameterization to explicitly represent deposition and condensation freezing processes within a specified temperature range.(Chen et al., 2019)~~The number concentration of ice nuclei produced by deposition and condensation freezing, Nicenud ($m^{-3}$), is calculated as follows:~~The parameterization scheme selected here is developed by Jiang et al. (2016) and (Chen et al., 2019). It first developed by Jiang et al. (2016) based on dust events observed in Xinjiang, Huangshan, and Nanjing in China, using the static vacuum vapor diffusion chamber Frankfurt Ice nucleation Deposition freezing Experiment. Then some parameters of it was refined and extended it to represent both deposition and immersion freezing by Chen et al. (2019) . The number concentration of ice nuclei, $N_{icenud}$ by both deposition and condensation freezing is as the following:~~

$$Nicenud~~N_{icenud}(m^{-3})~~ = 5.7 * 10^{-7} n_{aer,0.5}^{0.018(273.16-Tk)-0.007S_i+0.342} * (273.16 - Tk)^{3.745} * S_i^{1.31} \quad (3)$$

~~$* (273.16 - Tk)^{3.745} * S_i^{1.31}$~~



带格式的

带格式的: 缩进: 首行缩进: 0 字符

带格式的 ...

域代码已更改 ...

带格式的: 字体: 10.5 磅

带格式表格

带格式的: 字体: 12 磅

带格式的 ...

带格式的: 字体: 12 磅

带格式的 ...

带格式的: 字体: 非倾斜

Where, $S_i$ is supersaturation with respect to ice.

WDM6 uses the formula $\rho q_{I0}$ ~~$(kg\ m^{-3})$~~=$(kg\ m^{-3})$= $4.92 \times 10^{-11} N_{ice}^{1.33}$ and ~~$P_{igen}$~~Pigen~~$(kg\ kg^{-1}\ s^{-1})$~~$(kg\ kg^{-1}\ s^{-1})$= $\frac{(q_{I0}-q_I)}{\Delta t}$ to calculate newly nucleation of ice. Where, ρ ~~ρ~~ denotes the newly-formed air density, and $q_{I0}$ is the predicted ice mixing ratio $(kg\ kg^{-1})$ ~~$(kg\ kg^{-1})$~~. Δt is the integration time step. Production rate for heterogeneous nucleation is calculated as the difference between $q_{I0}$ and the current ice mixing ratio ($q_I$). However, it does not account for the influence of nucleated IN size or the specific characteristics of different heterogeneous ice nucleation mechanisms on ice crystal development.

Here, the mass production rate of cloud ice newly nucleated is calculated as the following:

$$Pinud\ P_{inud}\ (kg\ kg^{-1}\ s^{-1}) = \frac{4}{3}\pi\frac{\rho_i}{\rho_a}\left(r_{df}^3 N_{icenud}\right)/\Delta t \quad (4)$$

$$Pinui\ P_{inui}\ (kg\ kg^{-1}\ s^{-1}) = \frac{4}{3}\pi\frac{\rho_i}{\rho_a}\left(r_{if}^3 N_{icenui}\right)/\Delta t$$

Where, ~~$P_{inud}$~~ Pinud $(kg\ kg^{-1}\ s^{-1})$ is mass production rate for deposition/condensation freezing, Pinui $(kg\ kg^{-1}\ s^{-1})$ ~~$P_{inui}$~~ is for immersion freezing. Pinud ~~$P_{inud}$~~ depletes water vapor to form cloud ice, while Pinui ~~$P_{inui}$~~ depletes cloud water to form cloud ice. $\rho_i$ is 500 $kg\ m^{-3}$ ~~$kg\ m^{-3}$ (Park and Lim, 2023)~~ (Park and Lim, 2023). $r_{if}$ represents the initial radius of cloud ice formed via immersion freezing, while $r_{df}$ represent the initial radius of cloud ice formed through deposition and condensation freezing, respectively. Δt is the integration time step. In the new online scheme, production rate for nucleated IN number concentration (Nigen) ~~($N_{igen}$)~~ is the sum of Nicenui a~~$N_{icenud}$~~nd Nicenud.~~and $N_{icenud}$~~.

The typical range of ice crystal radius in East Asia is about 10–100 μm (Chen et al., 2021), droplet radius range is about 1~30 μm (Um et al., 2018; Yang et al., 2021). Considering ice crystals generally grow from smaller particles and the radius of initial ice crystal size are often smaller than observed values, and with reference to the bin sizes of aerosol particles in CUACE (Um et al., 2018; Chen et al., 2021; Yang et al., 2021), this study assumes the characteristic radius of ice crystals ~~the ice crystal radius~~

带格式的: 上标
带格式的
带格式的: 字体: 12 磅
带格式的: 居中, 缩进: 首行缩进: 2 字符
带格式的
带格式的: 字体: 12 磅
带格式的
带格式的: 行距: 1.5 倍行距
带格式的
带格式的: 字体: 12 磅
带格式的: 字体: 12 磅
带格式的: 非突出显示
域代码已更改
带格式的: 非突出显示
带格式的
带格式的
域代码已更改

of $r_{df}$ and $r_{if}$ to be:

$$\begin{cases} r_{df=10\ \mu m(r_{aer}<10\ \mu m)} = 10\ \mu m(r_{aer} < 10\ \mu m) \\ r_{df=30\ \mu m(r_{aer}>10\ \mu m)} = 30\ \mu m(r_{aer} > 10\ \mu m) \end{cases} \quad (5)$$

$$\begin{cases} r_{if=30\ \mu m\ (r_{aer}<10\ \mu m)} = 30\ \mu m\ \ (r_{aer} < 10\ \mu m) \\ r_{if=50\ \mu m\ (r_{aer}>10\ \mu m)} = 50\ \mu m\ \ (r_{aer} > 10\ \mu m) \end{cases}$$

Then, the original production rate for nucleation of ice from vapor PigenP$_{igen}$ in WDM6 is replaced by the P$_{inud}$ aPinud and PinuiP$_{inui}$ described above.

带格式的: 字体: 非倾斜

带格式的: 字体: 12 磅

带格式的: 字体: 12 磅

### 2.4 Case description and test design

**The typical dust affected precipitation event**

The typical dust affected precipitation event is from 00:00 UTC on 9 April to 00:00 UTC on 15 April 2018, which contains two dust storms events in East Asia. One is from 9 to 11 April, originating in Mongolia and affected northern China. Lots of dust storm phenomena are observed in Mongolia, while blowing dust and floating dust phenomena are reported in central and western Inner Mongolia, central Gansu, Ningxia, northern Shaanxi, most parts of Shanxi, southern Hebei, northern Henan, and western Shandong in China (see Fig. S1 for locations). Another event is from 13 to 14 April. It also gains with widespread dust storm phenomena in Mongolia and central Inner Mongolia, blowing or floating dust phenomena observed in central Inner Mongolia, northern Shanxi, Beijing, Tianjin, and northern Hebei in China. Between the two dust storm events, the precipitation occurred from west to eat covering most of northern China extending to the Yangtze River area, from 00:00 UTC on 12 April to 00:00 UTC on 15 April, concentrated in Shaanxi, Henan, southern Hebei, and along the Yangtze River in Sichuan, Hubei, Anhui, and the Jiangsu-Zhejiang-Shanghai area.

Figure 1a presents the dust-affected areas by dust phenomenon from Meteorological stations and $PM_{10}$ from the National Environmental Monitoring Network of the Ministry of Environmental Protection. Based on the distribution of dust in this event, the domain bounded by 90-135 °E and 20-54 °N is defined as the major dust-affected area (DA, region 1 outer red rectangle in Figure 1). Together with the real precipitation distribution (Fig. 5a), the domain bounded by 103°–130.5°E and 27.5°–

50°N is defined as the dust-affected precipitation (DP) area (DPA, region 2 in Figure 1). The whole model domain covers 70°–145°E and 15°–64.5°N, containing the DA and DPA. To investigate the impact of dust on precipitation in regions distant from the dust source in Section 3.3, we calculate horizontal hydrometeor fluxes across 116°E (33°–50°N) and 33°N (103°–116°E) during 12:00 UTC on 12 April to 18:00 UTC on 13 April (Fig. 6). The area bounded by 103°–116°E and 33°–50°N is defined as the near-dust-source area (NDSA, region 3 in Figure 1).

GRAPES/CUACE successfully reproduces both the spatial distribution and intensity of the dust events (Fig. 1b). Considering that many radar observations and model studies have indicated that dust mainly participates in heterogeneous ice nucleation as ice nuclei within the mid-tropospheric layer (-20 - 0 ℃) (Haarig et al., 2019; He et al., 2021; He et al., 2023), which corresponds to altitudes between 4 and 7 km in the present case, Fig. 1c shows the simulated dust concentration within this layer.

~~Considering that many radar observations and model studies have indicated that dust mainly participates in within the mid-tropospheric layer ( 20 - 0 ℃) between 4 and 7 km in altitude (Haarig et al., 2019; He et al., 2021; He et al., 2023), Fig. 1c also shows the simulated dust within this layer.~~

域代码已更改

域代码已更改

**Test design**

As shown in Table 1, two tests are designed. The first test uses the on-line aerosol–CCN–cloud interaction scheme from Zhou et al. (2016), denoted as T_CTL. Based on T_CTL, the second test adds the on-line aerosol-IN nucleation scheme described in Section 2.3, denoted as T_IN.

The successive integration is cut into several three-days-interval with a warm restart. It starts at 00:00 UTC on April 5, 2018 with 6 days spinning up for tracers in CUACE. As simulation time increases, integration errors tend to accumulate (Zhang et al., 2019), and to minimize the influence of initial conditions on precipitation, the simulations in this study were divided into several time segments: 5–8 April, 8–11 April, 11–14 April, and 13–16 April. Among these, the simulation results for 13 April were taken from the 11–14 April experiment to minimize the influence of initial conditions

域代码已更改

on precipitation development. Except for water vapor, all initial values of hydrometeors are zero for each run. The model outputs 1-hourly precipitation data. To compare with the observed 6-hourly precipitation, the model outputs are temporally interpolated to the time stamps of the observations.

The initial and boundary meteorological conditions for GRAPES/CUACE are from the Final Operational Global Analysis data produced jointly by the National Centers for Environmental Prediction (NCEP) and the National Center for Atmospheric Research (NCAR) at a temporal resolution of 6 hours and a spatial resolution of 0.15°. The anthropogenic emissions are from Multi-resolution Emission Inventory for China (Li et al., 2017).

域代码已更改

**2.5 Data and evaluation methodology**

The initial and boundary meteorological conditions for GRAPES/CUACE are obtained from the NCEP/NCAR Final Operational Global Analysis (FNL) data, with a temporal resolution of 6 hours and a spatial resolution of 0.25°. Dust observations are obtained from two sources: weather phenomena from the CMA surface meteorological observation network with a temporal resolution of 3 hours, while $PM_{10}$ and $PM_{2.5}$ concentration data from the national environmental monitoring network of the Ministry of Ecology and Environment of China, with a temporal resolution of 1 hour. 6-hour rainfall data are also from CMA surface meteorological observation network. As there are more than 2,000 precipitation stations in DA, only 63 stations of levels 1 and 2 are selected for evaluation, of which 43 stations are in DPA to avoid overfitting with the model outputs. Due to the complex sources of $PM_{10}$ and considering the relatively long atmospheric residence time of dust, we select precipitation stations where the $PM_{2.5}/PM_{10}$ ratio is less than 0.6 within 24 hours prior to the precipitation event as representative of dust-influenced precipitation (DP) stations (Wang and Yan, 2007; Filonchyk et al., 2019).

域代码已更改

Model performance is evaluated using mean absolute error (MAE), root mean square error (RMSE), and symmetric mean absolute percentage error (sMAPE) (Shcherbakov et al., 2013):

域代码已更改

$$MAE=\frac{\sum_{i=1}^{n}(r_{mi}-r_{oi})^2}{n} \quad (8)$$

$$RMSE=\sqrt{\frac{\sum_{i=1}^{n}(r_{mi}-r_{oi})^2}{n}}$$

$$sMAPE = \frac{1}{n}\sum_{i=1}^{n}\frac{|r_{mi}-r_{oi}|}{|r_{mi}|+|r_{oi}|}$$

$$aMAPE = \frac{r_{mi}-r_{oi}}{|r_{mi}|+|r_{oi}|}$$

where $r_{mi}$ represents the simulated cumulative precipitation at station i, and $r_{oi}$ denotes the observed precipitation. For MAE, RMSE and sMAPE, values closer to 0 indicate better simulation performance. The aMAPE is used to evaluate whether the simulated precipitation is overestimated or underestimated compared with the observation. When aMAPE > 0, the precipitation is overestimated; when aMAPE < 0, the precipitation is underestimated.

The horizontal hydrometeor fluxes shown in Section 3.3 are calculated using a grid-based mass transport formulation. For each model layer, the flux is computed as

$$F = \rho_{air} q_x V \Delta z \Delta s \quad (9)$$

where F is the hydrometeor flux (kg $s^{-1}$), $\rho_{air}$ is the air density (kg $m^{-3}$), $q_x$ is the mass mixing ratio of the hydrometeor species (kg $kg^{-1}$), V_n is the wind component normal to the cross section (m $s^{-1}$), $\Delta z$ is the layer thickness (m), and $\Delta s$ is the horizontal grid spacing along the cross section (m).

## 3 Results

### 3.1 Ice nuclei

During the DP event, the implemented on-line aerosol–IN nucleation scheme enables dust aerosols to modify the nucleated IN number concentration. Figures 2a and 2b show the horizontal distribution of the maximum nucleated IN number concentration between 4 and 7 km above ground level at DP stations during the time period from 00:00 UTC on 11 April to 00:00 UTC on 15 April 2018 for T_CTL and T_IN, respectively. Figure 2c presents the vertical distribution of DP-event-averaged production rate for Nigen for T_CTL (red line) and T_IN (blue line). Figure 2d presents



带格式的: 字体: 非倾斜
带格式的: 字体: 非倾斜
带格式的: 字体: 12 磅
带格式的: 字体: 12 磅, 字体颜色: 自动设置
带格式的: 字体: 12 磅
带格式的: 正文, 缩进: 左侧: 0 厘米
带格式的: 字体: 12 磅, 字体颜色: 自动设置
带格式表格
带格式的: 字体: (中文) +中文正文 (等线), 字体颜色: 自动设置
带格式的: 字体: 12 磅, 字体颜色: 自动设置
带格式的: 字体: 12 磅, 字体颜色: 自动设置
带格式的: 字体: 12 磅, 字体颜色: 自动设置
带格式的: 字体: 12 磅, 字体颜色: 自动设置
带格式的: 字体: 12 磅, 字体颜色: 自动设置
带格式的: 正文, 缩进: 左侧: 0 厘米
带格式的: 字体: 12 磅, 字体颜色: 自动设置
带格式的: 字体: 12 磅, 字体颜色: 自动设置
带格式的: 字体: 12 磅, 字体颜色: 自动设置
带格式的: 字体: 12 磅, 非突出显示
带格式的: 字体颜色: 自动设置

the vertical distribution of cloud ice mass production rate for heterogeneous ice nucleation for T_CTL and T_IN. Based on the variation characteristics, the vertical layer is divided into three parts: layer A, above 7 km (temperature below −18 °C); layer B, between 4 and 7 km (temperature approximately −18 °C to -1.5 °C); and layer C, below 4 km (temperature approximately -1.5 °C to 18 °C).

The on-line aerosol-IN nucleation scheme can correct the systematic underestimation of IN concentrations. The maximum nucleated IN number concentrations in T_CTL can reach $10^2$ $L^{-1}$ in layer B during the DP event (Fig. 2a), showing a relatively uniform horizontal pattern, which is much lower than observed IN concentrations ($10^2$–$10^4$ $L^{-1}$) during East Asian dust events (Bi et al., 2019; Tobo et al., 2019; Chen et al., 2021; Hu et al., 2023). For example, Chen et al. (2021) measured immersion-mode INPs at Peking University Atmosphere Environment Monitoring Station during spring 2018–2019 and found that dust periods increased INP concentrations by approximately two orders of magnitude, reaching $10^2$ $L^{-1}$ between −15℃ and −28℃.

The DP-event-averaged production rate for nucleated IN number concentration ranges 0.005-0.01 $L^{-1}$ ~~s~~$^{-1}$ in layer B (Fig. 2c). In T_CTL, the production rate for nucleated IN number concentration increases with height (Fig. 2c), primarily due to the temperature-dependent nature of original WDM6 scheme. As a result, cloud ice mass production rate due to heterogeneous ice nucleation peak near the −40 °C level (Fig. 2d). Above this layer, IN concentration continues to increase, but production rate of heterogeneously nucleated cloud ice begins to decline due to limited water vapor (Fig. 2d). In the real atmosphere, the number concentration of effective ice-nucleating particles often reaches a maximum in the mid-troposphere rather than at the highest altitudes (He et al., 2023), suggesting that the continuous increase of IN at higher altitudes in T_CTL may inconsistent with typical observed .

In T_IN, the maximum nucleated IN number concentrations can reach $10^4$ $L^{-1}$ in layer B during the DP event (Fig. 2b), closer to those observed or simulated in other East Asian dust events (Bi et al., 2019; Tobo et al., 2019; Chen et al., 2021; Hu et al.,

域代码已更改

带格式的: 非突出显示

带格式的: 字体: (中文) 宋体, 12 磅, 字体颜色: 自动设置

带格式的: 字体: (中文) 宋体, 12 磅, 字体颜色: 自动设置

带格式的: 字体: (中文) 宋体, 12 磅, 字体颜色: 自动设置

带格式的: 字体: (中文) 宋体, 12 磅, 字体颜色: 自动设置

带格式的: 字体: (中文) 宋体, 12 磅, 字体颜色: 自动设置

带格式的: 字体: (中文) 宋体, 12 磅, 字体颜色: 自动设置

带格式的: 字体: 12 磅

带格式的: 字体: (中文) 宋体, 字体颜色: 自动设置

域代码已更改

域代码已更改

2023). The DP-event-averaged production rate for nucleated IN number concentration ranges from 0.2 to 3.7 $L^{-1}$ ~~S~~$s^{-1}$ in layer B (Fig. 2c), and the cloud ice mass production rate for heterogeneous ice nucleation also peaks in this layer, which is consistent with radar observations and other modeling studies (Haarig et al., 2019; He et al., 2021; He et al., 2023). As immersion freezing is the dominant heterogeneous nucleation mechanism (DeMott et al., 2015; Hiranuma et al., 2015), this study compares the number concentration of ice-nucleating particles activated by immersion freezing with those activated by deposition and condensation freezing. The DP-event-averaged results indicate that the activated IN number concentration from immersion freezing exceeds that from deposition and condensation freezing by approximately 4–5 orders of magnitude.~~the production rate of IN produced by it can exceed that of deposition and condensation freezing by 4–5 orders and the production rate of cloud ice by 5–6 orders in DP-event-averaged.~~

域代码已更改

域代码已更改

带格式的: 字体: (中文) 宋体

### 3.2 Hydrometeors

During the DP event, the introduction of the on-line aerosol-IN nucleation scheme allows dust aerosols to alter the distribution of cloud hydrometeors. Figure 3 shows the DP-event-averaged vertical distributions of hydrometeors in T_CTL and T_IN, averaged over the dust–precipitation period (00 UTC 11 April–00 UTC 15 April 2018) and over dust–precipitation stations, as well as their difference (T_IN − T_CTL), by using budget analysis. Figure 4 shows the differences in the production rates of different hydrometeors (T_IN − T_CTL). To further examine the thermodynamic conditions responsible for the weakened production rate of cloud droplet activation from CCN in T_IN in Figure 4, the vertical profiles of temperature and water vapor were analyzed, averaged over the dust–precipitation stations in DPA and NDSA during the period when the dust impact was most pronounced (18:00 UTC 11 April to 18:00 UTC 12 April) (Figure 5).

带格式的: 非突出显示

带格式的: 字体: 10.5 磅

带格式的: 缩进: 首行缩进: 0 字符

**Cloud ice**

In layer A, when dust aerosols are considered, the IN number concentration

decreases in T_IN (Fig. 2c), resulting in cloud ice number concentrations in T_IN that are approximately 5 $L^{-1}$ lower than those in T_CTL, about 40% of T_CTL (Fig. 3d). The cloud ice mass concentration is reduced to only 10% – 50% of T_CTL (Fig. 3a,3b). Because the two primary processes contributing to cloud ice formation in this layer—heterogeneous nucleation and deposition-sublimation of cloud ice —are both suppressed (Fig. 4a), and the total production rate of cloud ice (Pigen+Pidep-Psaut-Praci-Psaci-Pgaci) drops to less than 24% of that in T_CTL. On the one hand, the nucleated IN number concentration decreases, weakening the Pigen in T_IN by 1–2 orders of magnitude relative to T_CTL. On the other hand, the reduction in cloud ice number concentration allows the ice crystals to grow more efficiently, with their effective particle size generally reaching 98%-135% of that in T_CTL. The combined effect of these two factors ultimately limits the deposition of water vapor onto the ice crystals. Consequently, Pidep decreases to 20%–50% of T_CTL, with the maximum suppression occurring at approximately 7–8 km (Fig. 4a).

In layer B, cloud ice number concentrations in T_IN range from 7 to 10 $L^{-1}$, approximately 120% of those in T_CTL. However, the cloud ice mass concentration in T_IN is reduced to only 70%–90% of T_CTL. The effective diameters of cloud ice also decrease to only 77%–97% of T_CTL, with occasional reductions exceeding 50%. This reduction is mainly attributable to combined effects of enhanced heterogeneous nucleation and suppressed depositional growth, and the total production rate of cloud ice drops to less than 82% of that in T_CTL. Dust aerosols provide additional ice nuclei, leading to a substantial enhancement of heterogeneous nucleation in T_IN and the formation of a much larger number of newly formed small ice crystals, with Pigen exceeding that in T_CTL by more than two orders of magnitude. However, the increase in cloud ice number concentration is accompanied by a reduction in individual particle size, which limits the deposition of water vapor onto ice crystals. This effect is combined with a decrease in relative humidity over dust–precipitation stations in the DPA (Fig. 5c), further inhibiting the deposition process. –As a result, Pidep in T_IN is reduced to about 30% of that in T_CTL, indicating that growth of cloud ice via

带格式的: 非突出显示

depositional processes is inhibited.

**Snow**

In layer A, the total snow production rate in T_IN increases to approximately 88% -200% of that in T_CTL (Psdep+Paacw+Psaut+Piacr+Praci+Psaci+Psacr-Pgaut-Pracs, Fig. 4b), leading to an increase in snow mass concentration to 120%–200% of T_CTL (Fig. 3a, 3b). This increase results from the combined effects of enhanced production rate for deposition-sublimation of snow (Psdep) and weakened production rate for aggregation of cloud ice to snow (Psaut) and production rate for accretion of cloud ice by snow (Psaci). The Psdep can reach approximately 2–5 times that in T_CTL (Fig. 4b). In WDM6, the deposition growth of ice-phase hydrometeors is constrained by the available water vapor, with cloud ice deposition given priority and snow deposition consuming the remaining vapor. Because Pidep is reduced to about 20%–50% of that in T_CTL, more water vapor is allocated to snow deposition, Psdep is then enhanced. Meanwhile, as cloud ice reduces, Psaut and Psaci are weakened in T_IN, with both processes reduced to approximately 40%–60% of their values in T_CTL (Fig. 4a, 4b). Despite the suppression of these source terms, the substantial enhancement of snow deposition growth dominates the snow budget in layer A, resulting in a net increase in snow production and cloud-snow mass concentration.

Finally, the ratio of cloud ice to cloud snow changes from 1:1 to 1:3 in layer A, more closely consistent with observation, which shows that cloud ice generally has higher number concentrations but lower mass concentrations than cloud snow (Gao et al., 2020; Yang et al., 2021; Feng et al., 2021; Fang et al., 2022). In the aircraft observations reported, small ice particles (>50 μm) reached concentrations of up to 300 $L^{-1}$, whereas large ice crystals (>600 μm) were only about 3 $L^{-1}$(Wang et al., 2023). Despite their much lower number concentrations, the larger particles contributed more to the ice mass because of their substantially greater sizes. In the present simulation, the cloud ice number concentrations in T_IN reach on the order of $10^1$ $L^{-1}$ in the main

带格式的: 缩进: 首行缩进: 0 字符

带格式的: 字体: 12 磅

带格式的: 正文, 缩进: 左侧: 0 厘米, 首行缩进: 2 字符

带格式的: 字体: (默认) Times New Roman, (中文) 宋体, 12 磅, 非突出显示

带格式的: 字体: 12 磅, 非突出显示

带格式的: 字体: 12 磅, 上标, 非突出显示

带格式的: 字体: 12 磅, 非突出显示

带格式的: 字体: 12 磅, 上标, 非突出显示

带格式的: 字体: 12 磅, 非突出显示

mixed-phase layer, which is substantially higher than in T_CTL and closer to the observed magnitudes, although still lower than some aircraft measurements.

带格式的: 字体: (中文) 宋体, 非突出显示

In layer B, the snow mass concentration shows relatively small changes, ranging from approximately 90% to 100% of T_CTL. From the perspective of cloud microphysics, the mechanisms are similar to those in layer A. Despite the reduction of Pidep, the Psdep increases to 130%–200% of T_CTL. At the same time, the decrease in cloud ice mass leads to the continued suppression of Psaut and Psaci, resulting in a total snow production rate of about 95% of T_CTL.

In layer C, although the model diagnostics indicate an enhancement in cloud-snow production processes (production rate for accretion of rain by snow (Psacr) and production rate for accretion of rain by cloud ice (Piacr)) and a reduction in the production rate for accretion of snow by rain (Pracs), newly formed cloud snow cannot be maintained because the temperature is already above 0 °C which makes it instantaneously melt, rapidly converting to rain. As a result, there is no significant change in snow mass concentration in this layer.

**Cloud water and rainwater**

Cloud water and rainwater are mainly distributed in layer C (temperature approximately -2 °C to 18 °C). In this layer, both cloud-water and rainwater mixing ratios in T_IN are about 90%-95% of those in T_CTL. This small reduction is primarily attributed to a weakening of the production rate for cloud droplet activation from CCN (Pcact), which decreases by about 5% in T_IN relative to T_CTL, indicating a suppressed conversion of water vapor into liquid water. As a consequence of the reduced cloud-water content, the production rate for accretion of rainwater by cloud water (Pracw) is also weakened, by 5%–10%. Meanwhile, the conversion of rainwater into ice-phase hydrometeors (Psac~~i~~r, ~~Pgaci~~Pgacr, and ~~Piaci~~Piacr) is enhanced. However, under the thermodynamic conditions of layer C, temperatures exceed the melting thresholds of ice-phase hydrometeors, the newly formed snow and graupel rapidly melt and are easily converted back into rainwater. Consequently, these ice-phase conversion processes contribute only marginally to the net change in rainwater mixing ratio.

Fig 5 show that, over dust–precipitation stations in both the NDSA and the DPA, the introduction of the on-line aerosol–IN nucleation scheme leads to temperature increases below 4 km, with changes of about 0.16 to 0.52 K, while the water vapor mixing ratio changes by –0.04 to 0.2 g $kg^{-1}$ during this 18:00 UTC 11 April to 18:00 UTC 12 April. These changes lead to a decrease in relative humidity within the warm-cloud layer. The relative humidity averaged over the dust–precipitation stations decreases by up to about 3 percentage points in the DPA during this period. In the NDSA, it locally reaches reductions of 6–7 percentage points around 4 km at 06:00 UTC 12 April. The reduced relative humidity suppresses droplet activation and condensational growth, thereby inhibiting the development of warm clouds in T_IN compared to T_CTL.

Overall, dust suppresses cloud development, reducing the total ice-phase hydrometeor content in layer A to 70 – 85% of T_CTL, the total ice-phase hydrometeor content in layer B to 85 – 91% of T_CTL, and the liquid-phase hydrometeor content in layer C to 90 – 95% of T_CTL. Our results indicate that dust aerosols tend to suppress cloud development in springtime dust-related precipitation over East Asia, where precipitation is predominantly stratiform. Similar suppression effects have also been reported in previous observational studies (Zhu et al., 2023).

### 3.3 Precipitation

The on-line aerosol–IN nucleation scheme can modulate the spatial distribution of precipitation. Figure ~~5~~6a shows the observed event-accumulated precipitation of DPA stations, and Figure ~~5~~6b shows the simulated event-accumulated precipitation of T_CTL. In T_CTL, 18 of 43 stations in DPA exhibit overestimated simulation precipitation compared to observations (overestimated stations), primarily located in areas near dust sources area such as Gansu, Ningxia, Shaanxi, and Inner Mongolia, as well as northeastern provinces including Shandong, Liaoning, Jilin, and Heilongjiang (Fig.~~5~~6b). At these overestimated stations, the observed mean accumulated precipitation is 11.49 mm, while the simulated mean accumulated precipitation is 25.55 mm (Fig.~~6~~7), with an average sMAPE of 45 %. The other 25 stations show

带格式的: 字体: (中文) 宋体, 12 磅, 非加粗, 非突出显示
带格式的: 非突出显示
带格式的: 非突出显示
带格式的: 非突出显示
带格式的: 字体: (默认) Times New Roman
带格式的: 非突出显示
带格式的: 非突出显示
带格式的: 非突出显示
带格式的: 字体: (默认) Times New Roman, (中文) 宋体, 12 磅, 字体颜色: 自动设置, 图案: 清除
带格式的: 非突出显示
带格式的: 非突出显示
带格式的: 字体: (默认) Times New Roman, (中文) 宋体, 12 磅, 字体颜色: 自动设置, 图案: 清除
带格式的: 字体: 10.5 磅
域代码已更改

underestimated simulated precipitation compared to observations (underestimated stations), mainly distributed across Hebei, Beijing, Henan, and the Yangtze River Basin downwind area of the dust events (Fig.~~5~~6b). At underestimated stations, the observed mean accumulated precipitation is 31.58 mm (Fig.~~6~~7), while the simulated value is only 4.63 mm, with an average sMAPE of −64 %.

In T_IN, the on-line aerosol–IN nucleation scheme does not alter the overall pattern of overestimation precipitation north of 35° N and underestimation precipitation to south of 35° N in T_CTL (Fig. ~~5~~6d). However, compared to T_CTL, notable improvements are mainly observed primarily between 34° and 40° N. This is driven by the process discussed in Section 3.2, where the presence of dust in layer C suppresses Pcact, thereby reducing the overestimation of precipitation near the dust source areas. sMAPE is reduced by about 1–10 % in areas near the dust source area, resulting in more accurate forecasts compared to both T_CTL (Fig. ~~5~~6e, f).

Rather than being removed by precipitation or evaporation, the suppressed cloud hydrometeors are transported downstream in T_IN. We calculate horizontal hydrometeor fluxes across 116°E, 33°–50°N and 33°N, 103°–116°E from 12:00 UTC on 12 April to 18:00 UTC on 13 April (Fig. ~~6~~7). Over the entire 0–12 km layer, the total hydrometeor flux slightly increases to about 102% of that in T_CTL.

Within the temperature range from 0 to -40 ℃, the total horizontal hydrometeor flux decreases by about 11 %, primarily due to a substantial reduction in cloud ice flux, accompanied by increases in snow and graupel fluxes. In Layer A, the total hydrometeor flux is about $4.4 \times 10^{-5}$ kg $s^{-1}$, corresponding to about 75 % of T_CTL. Cloud ice flux drops sharply to about 8 % of T_CTL, while snow and graupel fluxes increase markedly to about 19.8 times and 7.8 times, respectively. In Layer B, the total hydrometeor flux is about $2.6 \times 10^{-6}$ kg $s^{-1}$, corresponding to about 93 % of T_CTL, with cloud ice flux reduced to about 28 % of T_CTL, and snow and graupel fluxes increased to about 2.3 times and about 1.8 times, respectively. At temperatures above 0 ℃, the total horizontal hydrometeor flux increases to about 106 % of T_CTL, with cloud water and rainwater fluxes increasing to about 115 % and about 108 %, respectively.

These results indicate that although dust suppresses cold-cloud development in the upper and mid-troposphere, it enhances the downstream transport of liquid-phase hydrometeors near and below the melting layer, enhancing downstream precipitation. Finally, for underestimation stations, the mean accumulated precipitation increases by 1.1 mm compared to T_CTL, and precipitation simulation improves by approximately 4 %, with little changes in MAE and RMSE (Fig. ~~7~~8b). For overestimated stations, the mean accumulated precipitation decreases by 4.5 mm compared to T_CTL, and precipitation simulations improves by approximately 40%, with MAE reduced by 1.4 and RMSE reduced by 4.1 (Fig. ~~7~~8a).

In summary, because the reduction in cloud water in the 0–4 km layer is relatively small, the corresponding decrease in rainwater reaching the surface is also limited. As a result, the on-line aerosol–IN nucleation scheme exerts only a weak influence on the total precipitation amount. Nevertheless, it can modulate the spatial and temporal distribution of precipitation, impressing overestimated and altering underestimation in a degree, which is consistent with the findings of Park and Lim (2023) and Su and Fung (2018b).

域代码已更改

**4 Conclusions and discussion**

In order to explore the impact of spring dust aerosols on precipitation, this study develop an on-line aerosol-IN nucleation scheme in the regional model GRAPES/CUACE. The model performance has been evaluated by a typical dust-precipitation event from 00:00 UTC on 9 April to 00:00 UTC on 15 April 2018.

Dust provides ice nuclei by heterogeneous nucleation during dust-precipitation event. The on-line aerosol–IN nucleation scheme significantly modifies nucleated IN concentration distributions. The original WDM6 scheme exhibits a systematic underestimation of ice nuclei concentrations, with nucleated IN concentrations can reach $10^2$ $L^{-1}$ between 4 and 7 km altitude during the dust-precipitation event, and abnormally increase with height due to the temperature-dependent formulation of original WDM6 scheme, peaking near the −40° C layer. With the on-line aerosol–IN nucleation scheme, IN concentrations can reach $10^4$ $L^{-1}$ ~~$10^4$ $L^{-1}$~~, so for the cloud ice

带格式的: 上标

mass production rate concentrated peaking at about the layer between 4 and 7 km in height, more closer to the observations

Dust can inhibit the development of clouds. Above 7 km, dust suppresses the growth rate of cloud ice (through both heterogeneous nucleation and deposition-sublimation rate of cloud ice), and the total production rate of cloud ice drops to less than 24% of that in T_CTL, promoting snow formation and ultimately reducing the total ice-phase hydrometeor content to 70–85% of T_CTL. Meanwhile, the total snow production rate in T_IN increases to approximately 88% - 200% of that in T_CTL, reducing total ice-phase hydrometeor content to 70 – 85% of T_CTL. Between 4 and 7 km height, dust enhances heterogeneous nucleation of cloud ice, but the new smaller particles suppress cloud ice and reduces the deposition rate, resulting in the total ice-phase hydrometeor content decreasing to 85–91% of T_CTL. Below 4 km in height, the relative humidity decreases by about 3 percentage points on average over the dust-precipitation stations in T_IN. This decrease in relative humidity limits the conversion of water vapor to cloud water and of cloud water to rain, reducing the liquid-phase hydrometeor content to 90–95% of that in T_CTL.

~~Below 4 km in height, dust slightly suppresses the conversion of water vapor to cloud water and of cloud water to rain, reducing the liquid-phase hydrometeor content to 90–95% of T_CTL.~~

The dust can also modulate the spatial distribution of precipitation even though the on-line aerosol–IN nucleation scheme cannot alter completely the overall pattern of overestimation precipitation north of 35° N and underestimation precipitation to the south of 35° N as seen in T_CTL. The on-line aerosol–IN nucleation scheme mitigates the overestimation of precipitation near dust source areas. For overestimated stations, the event-mean accumulated precipitation decreases by about 4.5 mm relative to T_CTL, with the MAE reduces by 1.4 and the RMSE reduces by 4.1. Meanwhile, the cloud hydrometeors suppressed by dust IN are not removed from the atmosphere; instead, they remain in the weather system and transported downstream as the air mass moves, thereby alleviating the underestimation of precipitation in downstream areas. In

带格式的: 非突出显示

带格式的: 非突出显示

带格式的: 字体: (默认) Times New Roman, (中文) 宋体, 12 磅, 字体颜色: 自动设置, 图案: 清除

带格式的: 非突出显示

带格式的: 字体: (默认) Times New Roman, (中文) 宋体, 12 磅, 字体颜色: 自动设置, 图案: 清除

stations where precipitation is previously underestimated, the mean accumulated precipitation increases by about 1.1 mm relative to T_CTL.

This study shows improvements of dust as IN on cloud and precipitation simulation by a comprehensive online aerosol-IN-cloud interaction scheme. Considering both CCN and IN effects, rather than CCN alone, improves precipitation simulations by up to approximately 40 %. Aerosol and clouds interactions are an old open question, but there are still many uncertainties, due to the complex mechanisms of both CCN and IN. Furthermore, the scarcity of real-time observations hinders the in-depth exploration of detailed microphysical processes and their underlying mechanisms. More cases in different seasons and different dusty cases are needed to perform in the future with more observations.

**Code/data availability**

All source code and data can be accessed by contacting the corresponding author Chunhong Zhou (zhouch@cma.gov.cn).

**Author contributions.**

JZ developed the on-line aerosol-IN nucleation scheme, conducted the data analysis, and wrote the original draft of this paper. CHZ developed the aerosol-CCN-cloud interaction scheme and the on-line aerosol-IN nucleation scheme, and reviewed and edited the manuscript, providing critical insights. XYS reviewed the manuscript. SLG ~~HW~~ reviewed the manuscript and provided general insight. HW ~~SLG~~ reviewed the manuscript. XYZ reviewed the manuscript and gave guidance on the data analysis. All authors have given approval to the final version of the paper.

**Competing interests**

The authors declare that they have no conflict of interest.

**Financial support.**

This study was jointly supported by the NSFC Project (42090030) ~~and~~, the National Key Project of the Ministry of Science and Technology of China (2022YFC3701205), Four-Dimensional Variational Quantitative Inversion of Carbon Dioxide Sources and

Sinks in the Ecosystem of the Sichuan Basin (2024JDHJ0058), A Study on the Integrated Simulation System for the Interaction Between Greenhouse Gases and Air Quality in Sichuan Province and the Science and Technology Development Fund of CAMS (2023KJ003).

**Acknowledgment.**

All figures in this study were produced by the open-source software of MeteoInfoLab from http://www.meteothink.org/index.html. The meteorological initial and boundary conditions for the modeling system were obtained from the China Meteorological Data Sharing Service System (http://data.cma.cn/data/cdcindex/cid/98c64da7ee348b37 html). The meteorological observations were obtained from the China Meteorological Data Sharing Service System (http://data.cma.cn/data/cdcindex/cid/f0fb4b55508804ca.html). The $PM_{10}$ and PM2.5 concentration data from the national environmental monitoring network of the Ministry of Ecology and Environment of China (http://www.cnemc.cn). The NCEP/NCAR Final Operational Global Analysis (FNL) data, with a temporal resolution of 6 hours and a spatial resolution of 0.25° (https://rda.ucar.edu/datasets/ds083.3/).

**References**

Albrecht, B. A.: Aerosols, Cloud Microphysics, and Fractional Cloudiness, Science, 245, 1227–1230, https://doi.org/10.1126/science.245.4923.1227, 1989.

Alfaro, S. and Gomes, L.: Modeling mineral aerosol production by wind erosion: Emission intensities and aerosol size distributions in source areas, Journal of Geophysical Research, 106, 18075–18084, https://doi.org/10.1029/2000JD900339, 2001.

Andreae, M. O. and Crutzen, P. J.: Atmospheric Aerosols: Biogeochemical Sources and Role in Atmospheric Chemistry, Science, 276, 1052–1058, https://doi.org/10.1126/science.276.5315.1052,1997.

Bi, K., McMeeking, G. R., Ding, D. P., Levin, E. J. T., DeMott, P. J., Zhao, D. L., Wang, F., Liu, Q., Tian, P., Ma, X. C., Chen, Y. B., Huang, M. Y., Zhang, H. L., Gordon, T. D., and Chen, P.: Measurements of Ice Nucleating Particles in Beijing, China, Journal of Geophysical Research: Atmospheres, 124, 8065–8075, https://doi.org/10.1029/2019JD030609, 2019.

Boose, Y., Welti, A., Atkinson, J., Ramelli, F., Danielczok, A., Bingemer, H. G., Plötze, M., Sierau, B., Kanji, Z. A., and Lohmann, U.: Heterogeneous ice nucleation on dust particles sourced from nine deserts worldwide – Part 1: Immersion freezing, Atmospheric Chemistry and Physics, 16, 15075–15095, https://doi.org/10.5194/acp-16-15075-2016, 2016.

Cantrell, W., Bunker, K., Niehaus, J., China, S., Woodward, X., Kostinski, A., and Mazzoleni, C.: Ice nucleation in the contact mode: Temperature and size dependence for selected dusts, AIP



带格式的: 非突出显示
带格式的: 字体: (默认) Times New Roman, (中文) 宋体, 12 磅
带格式的: 非突出显示
带格式的: 字体: (默认) Times New Roman
带格式的: 字体: (默认) Times New Roman
带格式的: 字体: (默认) Times New Roman
带格式的: 字体: (默认) Times New Roman
带格式的: 正文, 缩进: 左侧: 0 厘米, 悬挂缩进: 2 字符, 首行缩进: -2 字符
带格式的: 正文, 缩进: 左侧: 0 厘米, 悬挂缩进: 2 字符, 首行缩进: -2 字符

Conference Proceedings, 1527, 926, https://doi.org/10.1063/1.4803423, 2013.

Che, Y., Zhang, J., Zhao, C., Fang, W., Xue, W., Yang, W., Ji, D., Dang, J., Duan, J., Sun, J., Shen, X., and Zhou, X.: A study on the characteristics of ice nucleating particles concentration and aerosols and their relationship in spring in Beijing, Atmospheric Research, 247, 105196, https://doi.org/10.1016/j.atmosres.2020.105196, 2021.

Chen, D., Xue, J., Yang, X., Zhang, H., Shen, X., Hu, J., Wang, Y., Ji, L., and Chen, J.: New generation of multi-scale NWP system (GRAPES): General scientific design, Chinese Science Bulletin, 53, 3433–3445, https://doi.org/10.1007/s11434-008-0494-z, 2008.

Chen, J., Wu, Z., Chen, J., Reicher, N., Fang, X., Rudich, Y., and Hu, M.: Size-resolved atmospheric ice-nucleating particles during East Asian dust events, Atmospheric Chemistry and Physics, 21, 3491–3506, https://doi.org/10.5194/acp-21-3491-2021, 2021.

Chen, J., Wu, Z., Meng, X., Zhang, C., Chen, J., Qiu, Y., Chen, L., Fang, X., Wang, Y., Zhang, Y., Chen, S., Gao, J., Li, W., and Hu, M.: Observational evidence for the non-suppression effect of atmospheric chemical modification on the ice nucleation activity of East Asian dust, Sci Total Environ, 861, 160708, https://doi.org/10.1016/j.scitotenv.2022.160708, 2023.

Chen, Q., Yin, Y., Jiang, H., Chu, Z., Xue, L., Shi, R., Zhang, X., and Chen, J.: The Roles of Mineral Dust as Cloud Condensation Nuclei and Ice Nuclei During the Evolution of a Hail Storm, Journal of Geophysical Research Atmospheres, 124, https://doi.org/10.1029/2019JD031403, 2019.

DeMott, P. J., Prenni, A. J., Liu, X., Kreidenweis, S. M., Petters, M. D., Twohy, C. H., Richardson, M. S., Eidhammer, T., and Rogers, D. C.: Predicting global atmospheric ice nuclei distributions and their impacts on climate, Proceedings of the National Academy of Sciences, 107, 11217–11222, https://doi.org/10.1073/pnas.0910818107, 2010.

DeMott, P. J., Prenni, A. J., McMeeking, G. R., Sullivan, R. C., Petters, M. D., Tobo, Y., Niemand, M., Möhler, O., Snider, J. R., Wang, Z., and Kreidenweis, S. M.: Integrating laboratory and field data to quantify the immersion freezing ice nucleation activity of mineral dust particles, Atmospheric Chemistry and Physics, 15, 393–409, https://doi.org/10.5194/acp-15-393-2015, 2015.

Eastwood, M. L., Cremel, S., Gehrke, C., Girard, E., and Bertram, A. K.: Ice nucleation on mineral dust particles: Onset conditions, nucleation rates and contact angles, Journal of Geophysical Research: Atmospheres, 113, https://doi.org/10.1029/2008JD010639, 2008.

Fan, J., Leung, L. R., DeMott, P. J., Comstock, J. M., Singh, B., Rosenfeld, D., Tomlinson, J. M., White, A., Prather, K. A., Minnis, P., Ayers, J. K., and Min, Q.: Aerosol impacts on California winter clouds and precipitation during CalWater 2011: local pollution versus long-range transported dust, Atmospheric Chemistry and Physics, 14, 81–101, https://doi.org/10.5194/acp-14-81-2014, 2014.

Fang, W., Lou, X., Zhang, X., and Fu, Y.: Numerical Simulations of Cloud Number Concentration and Ice Nuclei Influence on Cloud Processes and Seeding Effects, Atmosphere, 13, 1792, https://doi.org/10.3390/atmos13111792, 2022.

Feng, Q., Niu, S., Niu, T., Fan, X., Shen, D., and Yang, J.: Aircraft—Based Observation of the Physical Characteristics of Snowfall Cloud in Shanxi Province, Chinese Journal of Atmospheric Sciences (in Chinese), 45, 1146–1160, https://doi.org/10.3878/j.issn.1006-9895.2106.21004 2021.

Filonchyk, M., Yan, H., Shareef, T. M. E., and Yang, S.: Aerosol contamination survey during dust

**带格式的:** 正文, 缩进: 左侧: 0 厘米, 悬挂缩进: 2 字符, 首行缩进: -2 字符

storm process in Northwestern China using ground, satellite observations and atmospheric modeling data, Theor Appl Climatol, 135, 119–133, https://doi.org/10.1007/s00704-017-2362-8, 2019.

Gao, Q., Guo, X., He, H., Liu, X., Huang, M., and Ma, X.: Numerical Simulation Study on the Microphysical Characteristics of Stratiform Clouds with Embedded Convections in Northern China based on Aircraft Measurements, Chinese Journal of Atmospheric Sciences(in Chinese), 44, 899–912, https://doi.org/10.3878/j.issn.1006-9895.1908.19114, 2020.

Gibbons, M., Min, Q., and Fan, J.: Investigating the impacts of Saharan dust on tropical deep convection using spectral bin microphysics, Atmospheric Chemistry and Physics, 18, 12161–12184, https://doi.org/10.5194/acp-18-12161-2018, 2018.

Gong, S. L. and Zhang, X. Y.: CUACE/Dust ? an integrated system of observation and modeling systems for operational dust forecasting in Asia, Atmospheric Chemistry and Physics, 8, 2333–2340, 2008.

Gong, S. L., Zhang, X. Y., Zhao, T. L., McKendry, I. G., Jaffe, D. A., and Lu, N. M.: Characterization of soil dust aerosol in China and its transport and distribution during 2001 ACE-Asia: 2. Model simulation and validation, Journal of Geophysical Research: Atmospheres, 108, https://doi.org/10.1029/2002JD002633, 2003.

Haarig, M., Ansmann, A., Walser, A., Baars, H., Urbanneck, C., Weinzierl, B., Schöberl, M., Dollner, M., Mamouri, R., and Althausen, D.: Estimation of dust related ice nucleating particles in the atmosphere: Comparison of profiling and in-situ measurements, E3S Web Conf., 99, 04002, https://doi.org/10.1051/e3sconf/20199904002, 2019.

He, C., Yin, Y., Huang, Y., Kuang, X., Cui, Y., Chen, K., Jiang, H., Kiselev, A., Möhler, O., and Schrod, J.: The Vertical Distribution of Ice-Nucleating Particles over the North China Plain: A Case of Cold Front Passage, Remote Sensing, 15, 4989, https://doi.org/10.3390/rs15204989, 2023.

He, Y., Zhang, Y., Liu, F., Yin, Z., Yi, Y., Zhan, Y., and Yi, F.: Retrievals of dust-related particle mass and ice-nucleating particle concentration profiles with ground-based polarization lidar and sun photometer over a megacity in central China, Atmospheric Measurement Techniques, 14, 5939–5954, https://doi.org/10.5194/amt-14-5939-2021, 2021.

Herbert, R. J., Murray, B. J., Dobbie, S. J., and Koop, T.: Sensitivity of liquid clouds to homogenous freezing parameterizations, Geophys. Res. Lett., 42, 1599–1605, https://doi.org/10.1002/2014GL062729, 2015.

Hiranuma, N., Augustin-Bauditz, S., Bingemer, H., Budke, C., Curtius, J., Danielczok, A., Diehl, K., Dreischmeier, K., Ebert, M., Frank, F., Hoffmann, N., Kandler, K., Kiselev, A., Koop, T., Leisner, T., Möhler, O., Nillius, B., Peckhaus, A., Rose, D., Weinbruch, S., Wex, H., Boose, Y., DeMott, P. J., Hader, J. D., Hill, T. C. J., Kanji, Z. A., Kulkarni, G., Levin, E. J. T., McCluskey, C. S., Murakami, M., Murray, B. J., Niedermeier, D., Petters, M. D., O'Sullivan, D., Saito, A., Schill, G. P., Tajiri, T., Tolbert, M. A., Welti, A., Whale, T. F., Wright, T. P., and Yamashita, K.: A comprehensive laboratory study on the immersion freezing behavior of illite NX particles: a comparison of 17 ice nucleation measurement techniques, Atmospheric Chemistry and Physics, 15, 2489–2518, https://doi.org/10.5194/acp-15-2489-2015, 2015.

Hong, S.-Y., Dudhia, J., and Chen, S.-H.: A Revised Approach to Ice Microphysical Processes for the Bulk Parameterization of Clouds and Precipitation, Monthly Weather Review, 132, 103–120, https://doi.org/10.1175/1520-0493(2004)132<0103:ARATIM>2.0.CO;2, 2004.

带格式的: 正文, 缩进: 左侧: 0 厘米, 悬挂缩进: 2 字符, 首行缩进: -2 字符

Hong, S.-Y., Noh, Y., and Dudhia, J.: A New Vertical Diffusion Package with an Explicit Treatment of Entrainment Processes, Monthly Weather Review, 134, 2318–2341, https://doi.org/10.1175/MWR3199.1, 2006.

Hu, Y., Tian, P., Huang, M., Bi, K., Schneider, J., Umo, N. S., Ullmerich, N., Höhler, K., Jing, X., Xue, H., Ding, D., Liu, Y., Leisner, T., and Möhler, O.: Characteristics of ice-nucleating particles in Beijing during spring: A comparison study of measurements between the suburban and a nearby mountain area, Atmospheric Environment, 293, 119451, https://doi.org/10.1016/j.atmosenv.2022.119451, 2023.

Igel, A. L., Igel, M. R., and Heever, S. C. van den: Make It a Double? Sobering Results from Simulations Using Single-Moment Microphysics Schemes, https://doi.org/10.1175/JAS-D-14-0107.1, 2015.

Ilotoviz, E., Khain, A. P., Benmoshe, N., Phillips, V. T. J., and Ryzhkov, A. V.: Effect of Aerosols on Freezing Drops, Hail, and Precipitation in a Midlatitude Storm, Journal of the Atmospheric Sciences, 73, 109–144, https://doi.org/10.1175/JAS-D-14-0155.1, 2016.

Jiang, H., Yin, Y., Su, H., Shan, Y., and Gao, R.: The characteristics of atmospheric ice nuclei measured at the top of Huangshan (the Yellow Mountains) in Southeast China using a newly built static vacuum water vapor diffusion chamber, Atmospheric Research, 153, 200–208, https://doi.org/10.1016/j.atmosres.2014.08.015, 2015.

Jiang, H., Yin, Y., Wang, X., Gao, R., Yuan, L., Chen, K., and Shan, Y.: The measurement and parameterization of ice nucleating particles in different backgrounds of China, Atmospheric Research, 181, 72–80, https://doi.org/10.1016/j.atmosres.2016.06.013, 2016.

Kang, J.-Y., Yoon, S., Shao, Y., and Kim, S.-W.: Comparison of vertical dust flux by implementing three dust emission schemes in WRF/Chem, Journal of Geophysical Research, 116, https://doi.org/10.1029/2010JD014649, 2011.

Kang, Y., Jin, S., Peng, X., Yang, X., Shang, K., and Wang, S.: Comparative Analysis of Single-Moment and Double-Moment Microphysics Schemes in WRF on the Torrential Rainfall Event in North China During 1921 July, 2016, Plateau Meteorology, 37, 481–494, 2018.

Kanji, Z. A., Ladino, L. A., Wex, H., Boose, Y., Burkert-Kohn, M., Cziczo, D. J., and Krämer, M.: Overview of Ice Nucleating Particles, https://doi.org/10.1175/AMSMONOGRAPHS-D-16-0006.1, 2017.

Kaufman, Y. J., Tanré, D., and Boucher, O.: A satellite view of aerosols in the climate system, Nature, 419, 215–223, https://doi.org/10.1038/nature01091, 2002.

Khain, A., Ovtchinnikov, M., Pinsky, M., Pokrovsky, A., and Krugliak, H.: Notes on the state-of-the-art numerical modeling of cloud microphysics, Atmospheric Research, 55, 159–224, https://doi.org/10.1016/S0169-8095(00)00064-8, 2000.

Knopf, D. A. and Alpert, P. A.: Atmospheric ice nucleation, Nat Rev Phys, 5, 203–217, https://doi.org/10.1038/s42254-023-00570-7, 2023.

Kumar, V. A., Pandithurai, G., Kulkarni, G., Hazra, A., Patil, S. S., Dudhambe, S. D., Patil, R. D., Chen, J.-P., and Niranjan, K.: Atmospheric ice nuclei concentration measurements over a high altitude-station in the Western Ghats, India, Atmospheric Research, 235, 104795, https://doi.org/10.1016/j.atmosres.2019.104795, 2020.

Lee, S. S., Kim, B.-G., Yum, S. S., Seo, K.-H., Jung, C.-H., Um, J. S., Li, Z., Hong, J., Chang, K.-H., and Jeong, J.-Y.: Effects of aerosol on evaporation, freezing and precipitation in a multiple cloud system, Clim Dyn, 48, 1069–1087, https://doi.org/10.1007/s00382-016-3128-1, 2017.

Li, J., Liu, W., Castarède, D., Gu, W., Li, L., Ohigashi, T., Zhang, G., Tang, M., Thomson, E. S., Hallquist, M., Wang, S., and Kong, X.: Hygroscopicity and Ice Nucleation Properties of Dust/Salt Mixtures Originating from the Source of East Asian Dust Storms, Front. Environ. Sci., 10, https://doi.org/10.3389/fenvs.2022.897127, 2022.

Li, M., Zhang, Q., Kurokawa, J., Woo, J.-H., He, K., Lu, Z., Ohara, T., Song, Y., Streets, D. G., Carmichael, G. R., Cheng, Y., Hong, C., Huo, H., Jiang, X., Kang, S., Liu, F., Su, H., and Zheng, B.: MIX: a mosaic Asian anthropogenic emission inventory under the international collaboration framework of the MICS-Asia and HTAP, Atmospheric Chemistry and Physics, 17, 935–963, https://doi.org/10.5194/acp-17-935-2017, 2017.

Liu, H., Yu, Y., Xia, D., Zhao, S., Ma, X., and Dong, L.: Analysis of the relationship between dust aerosol and precipitation in spring over East Asia using EOF and SVD methods, Science of The Total Environment, 908, 168437, https://doi.org/10.1016/j.scitotenv.2023.168437, 2024.

Marticorena, B. and Bergametti, G.: Modeling the atmospheric dust cycle: 1. Design of a soil-derived dust emission scheme, Journal of Geophysical Research: Atmospheres, 100, 16415–16430, https://doi.org/10.1029/95JD00690, 1995.

Mascioli, N. R., Evan, A. T., and Ralph, F. M.: Influence of Dust on Precipitation During Landfalling Atmospheric Rivers in an Idealized Framework, Journal of Geophysical Research: Atmospheres, 126, e2021JD034813, https://doi.org/10.1029/2021JD034813, 2021.

Molthan, A. L. and Colle, B. A.: Comparisons of Single- and Double-Moment Microphysics Schemes in the Simulation of a Synoptic-Scale Snowfall Event, https://doi.org/10.1175/MWR-D-11-00292.1, 2012.

Naeger, A. R.: Impact of dust aerosols on precipitation associated with atmospheric rivers using WRF-Chem simulations, Results in Physics, 10, 217–221, https://doi.org/10.1016/j.rinp.2018.05.027, 2018.

Nenes, A., Murray, B., and Bougiatioti, A.: Mineral Dust and its Microphysical Interactions with Clouds, Mineral Dust: A Key Player in the Earth System, 287–325, https://doi.org/10.1007/978-94-017-8978-3_12, 2014.

Niehaus, J., Becker, J. G., Kostinski, A., and Cantrell, W.: Laboratory Measurements of Contact Freezing by Dust and Bacteria at Temperatures of Mixed-Phase Clouds, https://doi.org/10.1175/JAS-D-14-0022.1, 2014.

Pan, X., Uno, I., Wang, Z., Nishizawa, T., Sugimoto, N., Yamamoto, S., Kobayashi, H., Sun, Y., Fu, P., Tang, X., and Wang, Z.: Real-time observational evidence of changing Asian dust morphology with the mixing of heavy anthropogenic pollution, Sci Rep, 7, 335, https://doi.org/10.1038/s41598-017-00444-w, 2017.

Park, S.-Y. and Lim, K.-S. S.: Implementation of Prognostic Cloud Ice Number Concentrations for the Weather Research and Forecasting (WRF) Double-Moment 6-Class (WDM6) Microphysics Scheme, Journal of Advances in Modeling Earth Systems, 15, e2022MS003009, https://doi.org/10.1029/2022MS003009, 2023.

Patnaude, R. J., McCluskey, C. S., Roberts, G. C., DeMott, P. J., Hill, T. C. J., McFarquhar, G. M., Kollias, P., Ranjbar, K., Wolde, M., and Kreidenweis, S. M.: Characteristics of Ice Nucleating Particles From the Long-Range Transport of Saharan Dust, Geophysical Research Letters, 52, e2024GL113365, https://doi.org/10.1029/2024GL113365, 2025.

Possner, A., Ekman, A. M. L., and Lohmann, U.: Cloud response and feedback processes in stratiform mixed-phase clouds perturbed by ship exhaust, Geophysical Research Letters, 44,

1964–1972, https://doi.org/10.1002/2016GL071358, 2017.

Pu, Z. and Lin, C.: Evaluation of double-moment representation of ice hydrometeors in bulk microphysical parameterization: comparison between WRF numerical simulations and UND-Citation data during MC3E, Geosci. Lett., 2, 11, https://doi.org/10.1186/s40562-015-0028-x, 2015.

Shao, Y., Ishizuka, M., Mikami, M., and Leys, J. F.: Parameterization of size-resolved dust emission and validation with measurements, Journal of Geophysical Research: Atmospheres, 116, https://doi.org/10.1029/2010JD014527, 2011.

Shcherbakov, M., Brebels, A., Shcherbakova, N. L., Tyukov, A., Janovsky, T. A., and Kamaev, V. A.: A survey of forecast error measures, World Applied Sciences Journal, 24, 171–176, https://doi.org/10.5829/idosi.wasj.2013.24.itmies.80032, 2013.

Shen, X., Shi, Y., Wang, H., Zhang, M., and Han, J.: Comparison of two double-moment cloud microphysics schemes in the GRAPES_Meso model on simulating a cold cloud process, byzh, 41, 336–347, https://doi.org/10.3969/j.issn.1004-9045.2022.03.010, 2022.

Shen, X., Mei, H., Wang, W., and Huang, W.: Numerical Simulation of Ice-Phase Processes Using a Double-Moment Microphysical Scheme and a Sensitivity Test of Ice Nuclei Concentration, CJAS, 39, 83–99, https://doi.org/10.3878/j.issn.1006-9895.1405.13310, 2024.

Stevens, R. G., Loewe, K., Dearden, C., Dimitrelos, A., Possner, A., Eirund, G. K., Raatikainen, T., Hill, A. A., Shipway, B. J., Wilkinson, J., Romakkaniemi, S., Tonttila, J., Laaksonen, A., Korhonen, H., Connolly, P., Lohmann, U., Hoose, C., Ekman, A. M. L., Carslaw, K. S., and Field, P. R.: A model intercomparison of CCN-limited tenuous clouds in the high Arctic, Atmospheric Chemistry and Physics, 18, 11041–11071, https://doi.org/10.5194/acp-18-11041-2018, 2018.

Stier, P., van den Heever, S. C., Christensen, M. W., Gryspeerdt, E., Dagan, G., Saleeby, S. M., Bollasina, M., Donner, L., Emanuel, K., Ekman, A. M. L., Feingold, G., Field, P., Forster, P., Haywood, J., Kahn, R., Koren, I., Kummerow, C., L'Ecuyer, T., Lohmann, U., Ming, Y., Myhre, G., Quaas, J., Rosenfeld, D., Samset, B., Seifert, A., Stephens, G., and Tao, W.-K.: Multifaceted aerosol effects on precipitation, Nat. Geosci., 17, 719–732, https://doi.org/10.1038/s41561-024-01482-6, 2024.

Stith, J. L., Ramanathan, V., Cooper, W. A., Roberts, G. C., DeMott, P. J., Carmichael, G., Hatch, C. D., Adhikary, B., Twohy, C. H., Rogers, D. C., Baumgardner, D., Prenni, A. J., Campos, T., Gao, R., Anderson, J., and Feng, Y.: An overview of aircraft observations from the Pacific Dust Experiment campaign, Journal of Geophysical Research: Atmospheres, 114, https://doi.org/10.1029/2008JD010924, 2009.

Su, L. and Fung, J. C. H.: Investigating the role of dust in ice nucleation within clouds and further effects on the regional weather system over East Asia – Part 1: model development and validation, Atmospheric Chemistry and Physics, 18, 8707–8725, https://doi.org/10.5194/acp-18-8707-2018, 2018a.

Su, L. and Fung, J. C. H.: Investigating the role of dust in ice nucleation within clouds and further effects on the regional weather system over East Asia – Part 2: modification of the weather system, Atmospheric Chemistry and Physics, 18, 11529–11545, https://doi.org/10.5194/acp-18-11529-2018, 2018b.

Tobo, Y., Adachi, K., DeMott, P. J., Hill, T. C. J., Hamilton, D. S., Mahowald, N. M., Nagatsuka, N., Ohata, S., Uetake, J., Kondo, Y., and Koike, M.: Glacially sourced dust as a potentially

significant source of ice nucleating particles, Nat. Geosci., 12, 253–258, https://doi.org/10.1038/s41561-019-0314-x, 2019.

Tobo, Y., Uetake, J., Matsui, H., Moteki, N., Uji, Y., Iwamoto, Y., Miura, K., and Misumi, R.: Seasonal Trends of Atmospheric Ice Nucleating Particles Over Tokyo, Journal of Geophysical Research: Atmospheres, 125, e2020JD033658, https://doi.org/10.1029/2020JD033658, 2020.

Trochkine, D., Iwasaka, Y., Matsuki, A., Yamada, M., Kim, Y.-S., Nagatani, T., Zhang, D., Shi, G.-Y., and Shen, Z.: Mineral aerosol particles collected in Dunhuang, China, and their comparison with chemically modified particles collected over Japan, Journal of Geophysical Research: Atmospheres, 108, https://doi.org/10.1029/2002JD003268, 2003.

Um, J., McFarquhar, G. M., Stith, J. L., Jung, C. H., Lee, S. S., Lee, J. Y., Shin, Y., Lee, Y. G., Yang, Y. I., Yum, S. S., Kim, B.-G., Cha, J. W., and Ko, A.-R.: Microphysical characteristics of frozen droplet aggregates from deep convective clouds, Atmospheric Chemistry and Physics, 18, 16915–16930, https://doi.org/10.5194/acp-18-16915-2018, 2018.

Wang, H., Gong, S. L., Zhang, H. L., Chen, Y., Shen, X. S., Chen, D. H., Xue, J. S., Shen, Y. F., and Jin, W. Z.: A new-generation sand and dust storm forecasting system GRAPES_CUACE/Dust: Model development, verification and numerical simulation, Chinese Science Bulletin, https://doi.org/10.1007/s11434-009-0481-z, 2010.

Wang, H., Zhang, X. Y., Wang, P., Peng, Y., Zhang, W. J., Liu, Z. D., Han, C., Li, S. T., Wang, Y. Q., Che, H. Z., Huang, L. P., Liu, H. L., Zhang, L., Zhou, C. H., Ma, Z. S., Chen, F. F., Ma, X., Wu, X. J., Zhang, B. H., and Shen, X. S.: Chemistry-Weather Interacted Model System GRAPES_Meso5.1/CUACE CW V1.0: Development, Evaluation and Application in Better Haze/Fog Prediction in China, Journal of Advances in Modeling Earth Systems, 14, e2022MS003222, https://doi.org/10.1029/2022MS003222, 2022.

Wang, J., Wang, T., Yasheng, D., Wang, X., Lei, Y., Li, X., Wang, Z., and Shi, B.: Modulations of dust aerosols on precipitation: Evidence from a typical heavy sandstorm event, Atmospheric Research, 304, 107411, https://doi.org/10.1016/j.atmosres.2024.107411, 2024.

Wang, W., Sheng, L., Jin, H., and Han, Y.: Dust aerosol effects on cirrus and altocumulus clouds in Northwest China, J Meteorol Res, 29, 793–805, https://doi.org/10.1007/s13351-015-4116-9, 2015.

Wang, Y. and Yan, Z.: Effect of Different Verification Schemes on Precipitation Verification and Assessment Conclusion, Meteorological Monthly, 33, 9 ( 53-61 ), https://doi.org/10.3969/j.issn.1000-0526.2007.12.008, 2007.

Wang, Y., Kong, R., Cai, M., Zhou, Y., Song, C., Liu, S., Li, Q., Chen, H., and Zhao, C.: High small ice concentration in stratiform clouds over Eastern China based on aircraft observations: Habit properties and potential roles of secondary ice production, Atmospheric Research, 281, 106495, https://doi.org/10.1016/j.atmosres.2022.106495, 2023.

Xu, G. Q., Chen, D. H., Xue, J. S., Sun, J., and Wang, S. Y.: The program structure designing and optimizing tests of GRAPES physics, Chinese Science Bulletin, 53, 7, https://doi.org/10.1007/s11434-008-0418-y, 2008.

Yang, J., Hu, X., Lei, H., Duan, Y., Lv, F., and Zhao, L.: Airborne Observations of Microphysical Characteristics of Stratiform Cloud Over Eastern Side of Taihang Mountains, Chinese Journal of Atmospheric Sciences, 45(1), 88−106, 2021.

Yang, L., Yin, Y., Yang, S., Jiang, H., Xiao, H., Chen, Q., Su, H., and Chen, C.: Measurement and Analysis of Atmospheric Ice Nuclei in Nanjing, CJAS, 37, 579–594,

https://doi.org/10.3878/j.issn.1006-9895.2012.11242, 2013.

Zhang, M., Yu, H., Guo, J., Shen, X., Su, Y., Xue, H., and Dou, B.: Assessment on Unsystematic Errors of GRAPES_GFS 2.0, Journal of Applied Meteorological Science, 30, 332–344, 2019.

Zhang, W., Wang, H., Zhang, X., Huang, L., Peng, Y., Liu, Z., Zhang, X., and Che, H.: Aerosol–cloud interaction in the atmospheric chemistry model GRAPES_Meso5.1/CUACE and its impacts on mesoscale numerical weather prediction under haze pollution conditions in Jing–Jin–Ji in China, Atmospheric Chemistry and Physics, 22, 15207–15221, https://doi.org/10.5194/acp-22-15207-2022, 2022.

Zhang, Z. and Shen, X.: On the development of the GRAPES——A new generation of the national operational NWP system in China, Chinese Science Bulletin, 53, 4, https://doi.org/10.1007/s11434-008-0462-7, 2008.

Zhao, X., Lin, Y., Luo, Y., Qian, Q., Liu, X., Liu, X., and Colle, B. A.: A Double-Moment SBU-YLIN Cloud Microphysics Scheme and Its Impact on a Squall Line Simulation, Journal of Advances in Modeling Earth Systems, 13, e2021MS002545, https://doi.org/10.1029/2021MS002545, 2021.

Zhou, C., Zhang, X., Gong, S., Wang, Y., and Xue, M.: Improving aerosol interaction with clouds and precipitation in a regional chemical weather modeling system, Atmospheric Chemistry and Physics, 16, 145–160, https://doi.org/10.5194/acp-16-145-2016, 2016.

Zhou, C., Gui, H., Hu, J., Ke, H., Wang, Y., and Zhang, X.: Detection of New Dust Sources in Central/East Asia and Their Impact on Simulations of a Severe Sand and Dust Storm, Journal of Geophysical Research: Atmospheres, 124, 10232–10247, https://doi.org/10.1029/2019JD030753, 2019.

Zhou, C., Rao, X., Sheng, L., Zhang, J., Lu, Lin, J., Hu, J., Zhang, B., and Xu, R.: Application of Scale-adaptive Dust Emission Scheme to CMA-CUACE/Dust, yyqxxb, 35, 400–413, https://doi.org/10.11898/1001-7313.20240402, 2024.

Zhou, C. H., Gong, S. L., Zhang, X. Y., Wang, Y. Q., Niu, T., Liu, H. L., Zhao, T. L., Yang, Y. Q., and Hou, Q.: Development and evaluation of an operational SDS forecasting system for East Asia: CUACE/Dust, Atmospheric Chemistry and Physics, 8, 787–798, https://doi.org/10.5194/acp-8-787-2008, 2008.

Zhou, C.-H., Gong, S., Zhang, X.-Y., Liu, H.-L., Xue, M., Cao, G.-L., An, X.-Q., Che, H.-Z., Zhang, Y.-M., and Niu, T.: Towards the improvements of simulating the chemical and optical properties of Chinese aerosols using an online coupled model – CUACE/Aero, Tellus B: Chemical and Physical Meteorology, 64, 18965, https://doi.org/10.3402/tellusb.v64i0.18965, 2012.

Zhu, H., Li, R., Yang, S., Zhao, C., Jiang, Z., and Huang, C.: The impacts of dust aerosol and convective available potential energy on precipitation vertical structure in southeastern China as seen from multisource observations, Atmospheric Chemistry and Physics, 23, 2421–2437, https://doi.org/10.5194/acp-23-2421-2023, 2023.

## Figure

Figure 1

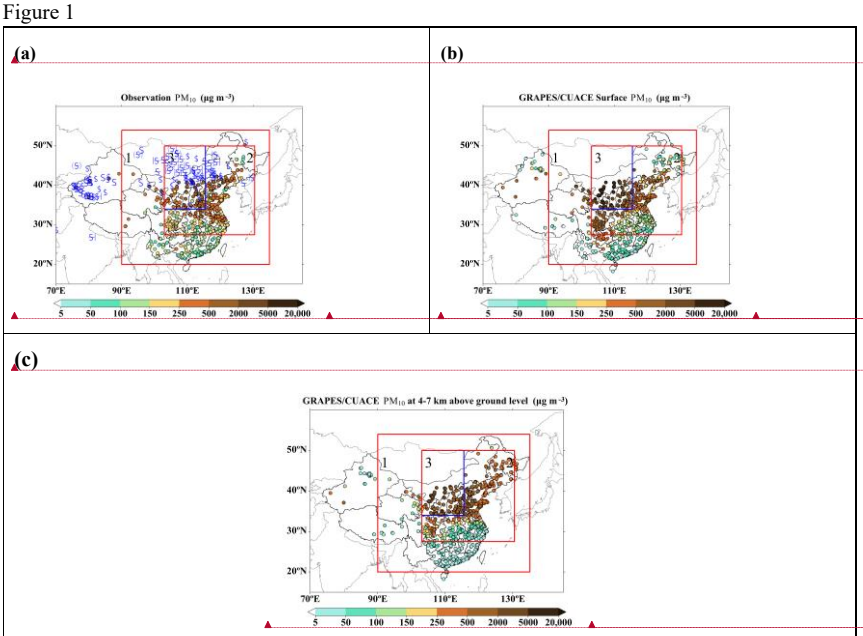


**Figure 1. Observed and simulated affected areas of the dust events from 11 to 15 April. (region 1 is DA; region 2 is DPA; region 3 is NDSA)**

**(a) Observed distribution of most sever dusty weather phenomena and maximum $PM_{10}$ concentration for each station during the test time;**

**(b) Same as (a) but for maximum $PM_{10}$ concentration by GRAPES/CUACE;**

**(c) Maximum $PM_{10}$ concentration distribution in the layer of 4-7 km in height by GRAPES/CUACE**

带格式的: 字体: (默认) Times New Roman

带格式的: 字体: (默认) Times New Roman

带格式的: 字体: (默认) Times New Roman

带格式的: 字体: (默认) Times New Roman

带格式的: 字体: (默认) Times New Roman

带格式的: 字体: (默认) Times New Roman

带格式的: 字体: (默认) Times New Roman

带格式的: 字体: (默认) Times New Roman

带格式的: 居中

带格式的: 字体: (中文) +中文正文 (等线), 9 磅, 加粗

带格式的: 字体: (默认) Times New Roman

带格式的: 字体: (默认) Times New Roman

带格式的: 字体: (默认) Times New Roman

Figure 2

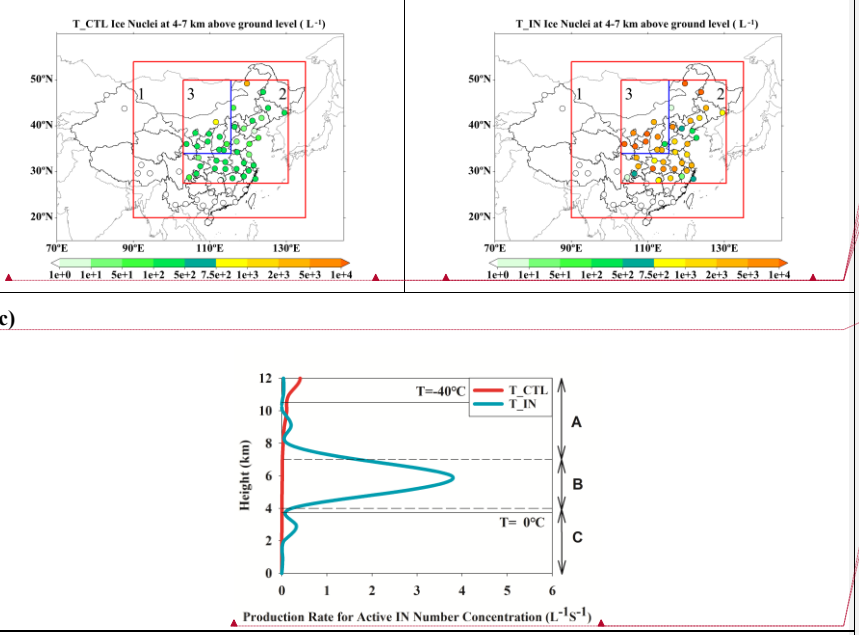


**Figure 2.** ~~distribution~~ Distribution **of IN from 11 to 15 April. (a) Maximum nucleated IN number concentration at 3-5 km altitude in T_CTL at DP stations; (b) Same as (a) but for T_IN simulations; (c) DP-event-averaged production rate for nucleated IN number concentration for T_CTL (red line) and T_IN (blue line)**

带格式的: 字体: (默认) Times New Roman

带格式的: 字体: (默认) Times New Roman

带格式的: 字体: (默认) Times New Roman

带格式的: 字体: (默认) Times New Roman

带格式的: 字体: (默认) Times New Roman

带格式的: 字体: (默认) Times New Roman

带格式的: 字体: (默认) Times New Roman

带格式的: 字体: (默认) Times New Roman

带格式的: 字体: (默认) Times New Roman

1010 Figure 3

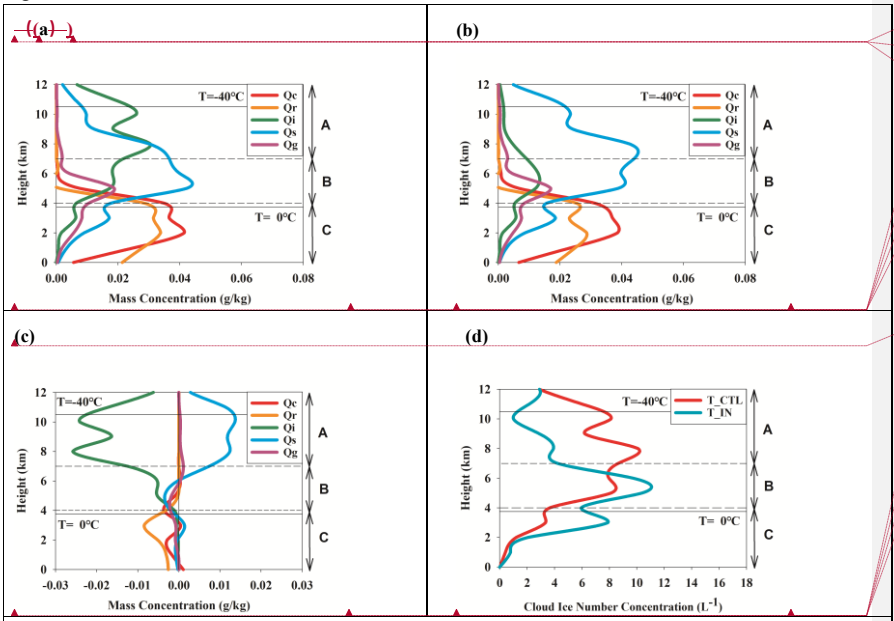


Figure 3. Distributions of hydrometeors, averaged over the dust–precipitation period (00 UTC 11 April–00 UTC 15 April 2018) and over dust–precipitation stations;~~Figure 3. DP event-averaged vertical distributions of hydrometeors:~~

**(a) hydrometeors simulated in T_CTL (b) hydrometeors simulated in T_IN**

**(c) hydrometeors difference by (T_IN- T_CTL);**

**(d) DP event-averaged vertical distributions of cloud ice number concentration**

带格式的: 字体: (默认) Times New Roman
带格式的: 字体: (默认) Times New Roman
带格式的: 字体: (默认) Times New Roman
带格式的: 字体: (默认) Times New Roman
带格式的: 字体: (默认) Times New Roman
带格式的: 字体: (默认) Times New Roman
带格式的: 字体: (默认) Times New Roman
带格式的: 字体: (默认) Times New Roman
带格式的: 字体: (默认) Times New Roman
带格式的: 字体: (默认) Times New Roman
带格式的: 字体: (默认) Times New Roman
带格式的: 字体: (默认) Times New Roman

Figure 4

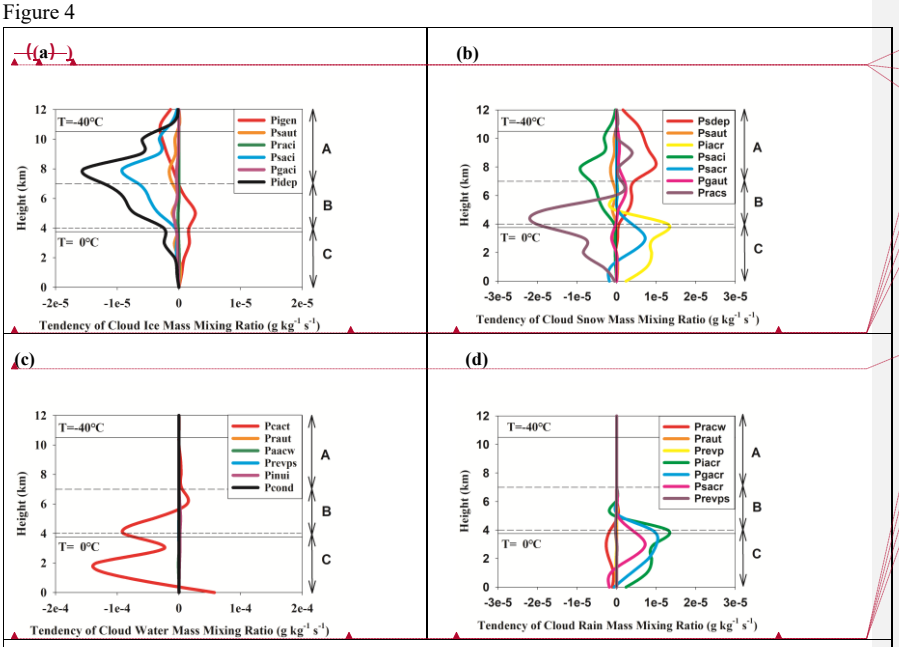


**Figure 4.** Vertical distributions of production rate difference for hydrometeors, averaged over the dust–precipitation period (00 UTC 11 April–00 UTC 15 April 2018) and over dust–precipitation stations; ~~DP event-averaged vertical distributions of production rate difference for hydrometeors:~~

**(a) production rate difference for cloud ice**

**(b) production rate difference for cloud snow**

**(c) production rate difference for cloud water**

**(d) production rate difference for cloud rain**

带格式的: 字体: (默认) Times New Roman
带格式的: 字体: (默认) Times New Roman
带格式的: 字体: (默认) Times New Roman
带格式的: 字体: (默认) Times New Roman
带格式的: 字体: (默认) Times New Roman
带格式的: 字体: (默认) Times New Roman
带格式的: 字体: (默认) Times New Roman
带格式的: 字体: (默认) Times New Roman
带格式的: 字体: (默认) Times New Roman
带格式的: 字体: (默认) Times New Roman
带格式的: 字体: (默认) Times New Roman
带格式的: 字体: (默认) Times New Roman
带格式的: 字体: (默认) Times New Roman
带格式的: 正文, 居中, 缩进: 左侧: 0 厘米, 首行缩进: 0 字符
带格式的: 字体: 9 磅, 加粗, 字体颜色: 自动设置
带格式的: 字体: (默认) Times New Roman
带格式的: 字体: (默认) Times New Roman

Figure 5

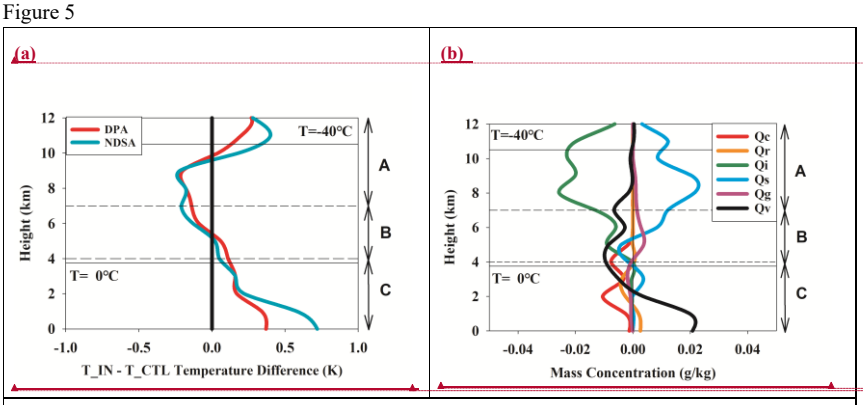


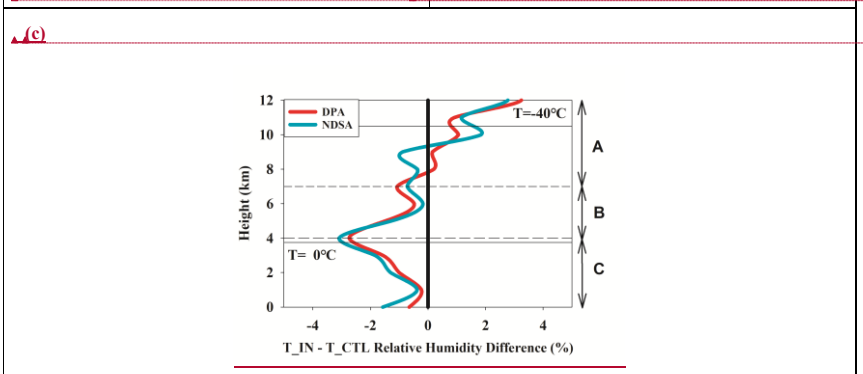


**Figure 5. Vertical distributions of temperature difference and relative humidity difference, averaged over dust–precipitation stations from 18:00 UTC 11 April to 18:00 UTC 12 April:**

**(a) Temperature difference (T_IN-T_CTL)**

**(b) Differences in hydrometeor and water vapor mixing ratios (T_IN − T_CTL). For clarity, the water vapor changes are scaled to one-tenth of their actual values.**

**(c) Relative humidity difference (T_IN-T_CTL)**

带格式的: 字体: (中文) +中文正文 (等线), 9 磅, 加粗, 字体颜色: 自动设置

带格式的: 字体: (中文) +中文正文 (等线), 9 磅, 加粗, 字体颜色: 自动设置

带格式的: 字体: (中文) +中文正文 (等线), 9 磅, 加粗, 字体颜色: 自动设置

带格式的: 字体: (中文) +中文正文 (等线), 9 磅, 加粗, 字体颜色: 自动设置

带格式的: 字体: (中文) +中文正文 (等线), 9 磅, 加粗, 字体颜色: 自动设置

带格式的: 字体颜色: 自动设置

带格式的: 字体: (中文) +中文正文 (等线), 9 磅, 加粗, 字体颜色: 自动设置

带格式的: 字体: (中文) +中文正文 (等线), 9 磅, 加粗, 字体颜色: 自动设置

Figure 6

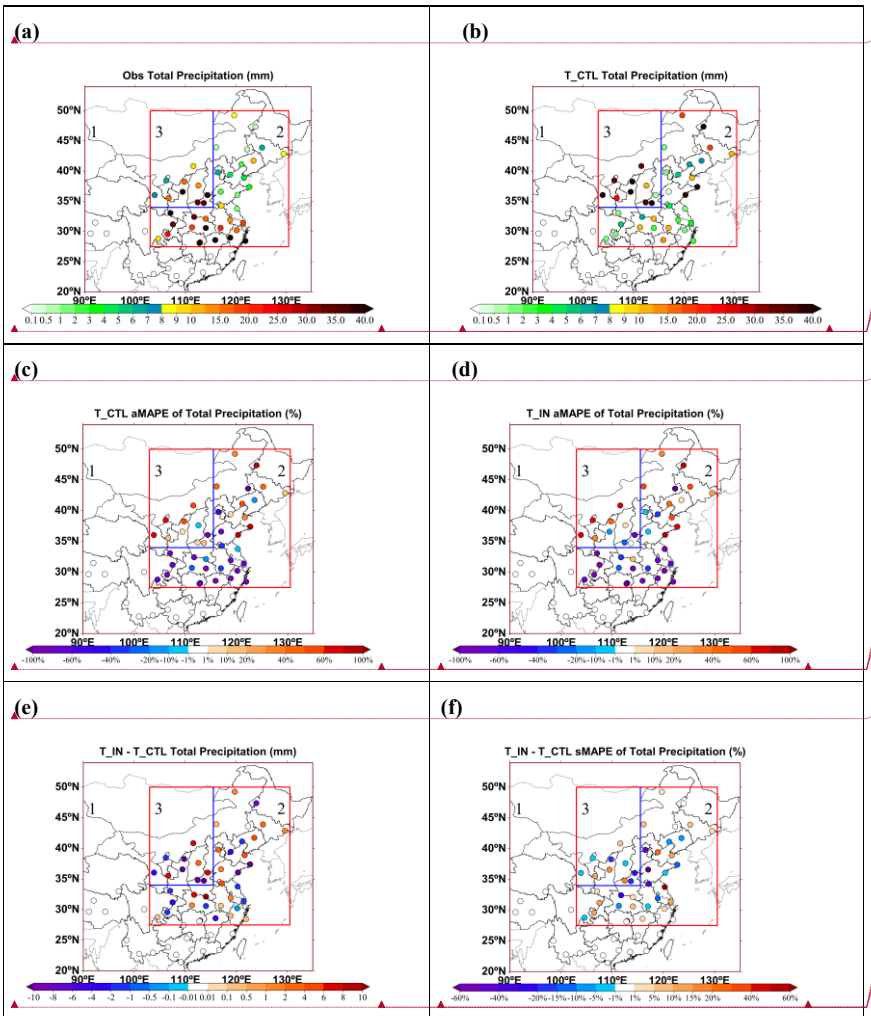


**Figure 56. Comparison of observed and simulated accumulated precipitation at dust-precipitation stations:**

**(a) Observed accumulated precipitation from 11th 00:00 UTC to 15th 00:00 UTC;**

**(b) Same as a but for T_CTL;**

**(c) aMAPE of simulated accumulated precipitation in T_CTL;**

**(d) aMAPE of simulated accumulated precipitation in T_IN;**

**(e) Difference in precipitation between T_IN and T_CTL;**

带格式的: 缩进: 左侧: 0 厘米, 首行缩进: 0 字符
带格式的: 字体: (默认) Times New Roman
带格式的: 字体: (默认) Times New Roman
带格式的: 字体: (默认) Times New Roman
带格式的: 字体: (默认) Times New Roman
带格式的: 字体: (默认) Times New Roman
带格式的: 字体: (默认) Times New Roman
带格式的: 字体: (默认) Times New Roman
带格式的: 字体: (默认) Times New Roman
带格式的: 字体: (默认) Times New Roman
带格式的: 字体: (默认) Times New Roman
带格式的: 字体: (默认) Times New Roman
带格式的: 字体: (默认) Times New Roman
带格式的: 字体: (默认) Times New Roman
带格式的: 字体: (默认) Times New Roman
带格式的: 字体: (默认) Times New Roman
带格式的: 字体: (默认) Times New Roman
带格式的: 字体: (默认) Times New Roman

**(f) Difference in sMAPE between T_IN and T_CTL.**

Figure 67

(a)

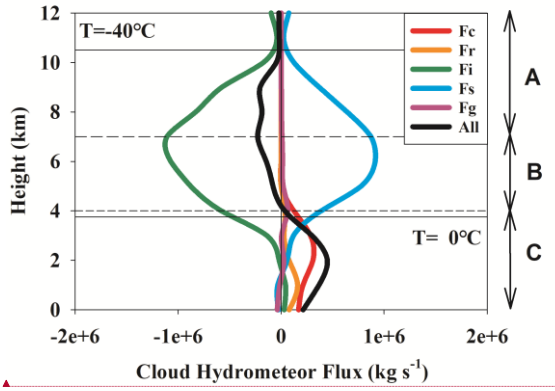


(b)

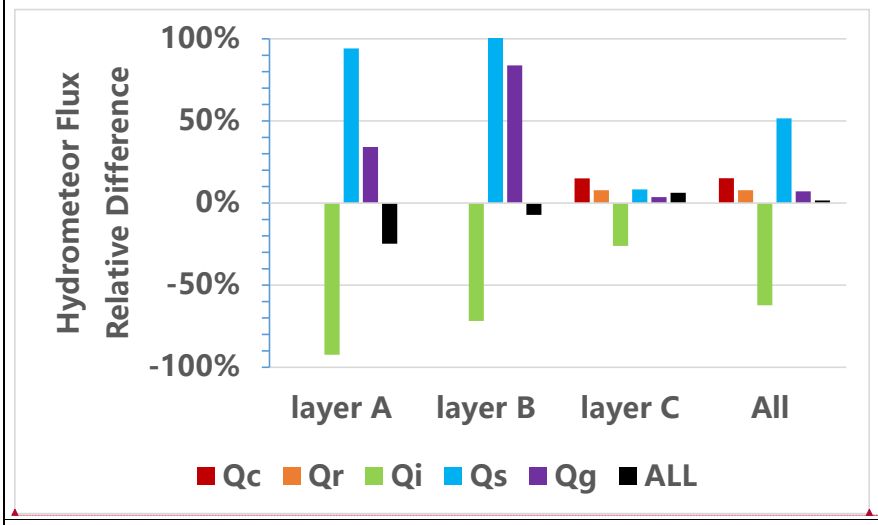


**Figure 67. Horizontal hydrometeor fluxes across 116°E (33°–50°N) and 33°N (103°–116°E).**

**Here, Fc denotes cloud water flux, Fr rainwater flux, Fi cloud ice flux, Fs snow flux, Fg graupel flux, and All the total hydrometeor flux.**

**(a) Differences in horizontal hydrometeor fluxes ~~{~~(T_IN − T_CTL)~~}~~.**

**(b) Fractional changes in horizontal hydrometeor fluxes in Layers A, B, C, and the total column, defined as (T_IN − T_CTL) / T_CTL. Snow and graupel fluxes in Layer A show extremely large increases (about**

带格式的: 字体: (默认) Times New Roman
带格式的: 字体: (默认) Times New Roman
带格式的: 字体: (默认) Times New Roman
带格式的: 字体: (默认) Times New Roman
带格式的: 字体: (默认) Times New Roman
带格式的: 字体: (默认) Times New Roman
带格式的: 字体: (默认) Times New Roman
带格式的: 字体: (默认) Times New Roman
带格式的: 字体: (默认) Times New Roman
带格式的: 字体: (默认) Times New Roman

**1883 % and 683 %, respectively); for better visualization, these values are scaled down by a factor of 20 in the figure.**

带格式的: 字体: (默认) Times New Roman

带格式的: 字体: (默认) Times New Roman

Figure ~~7~~8

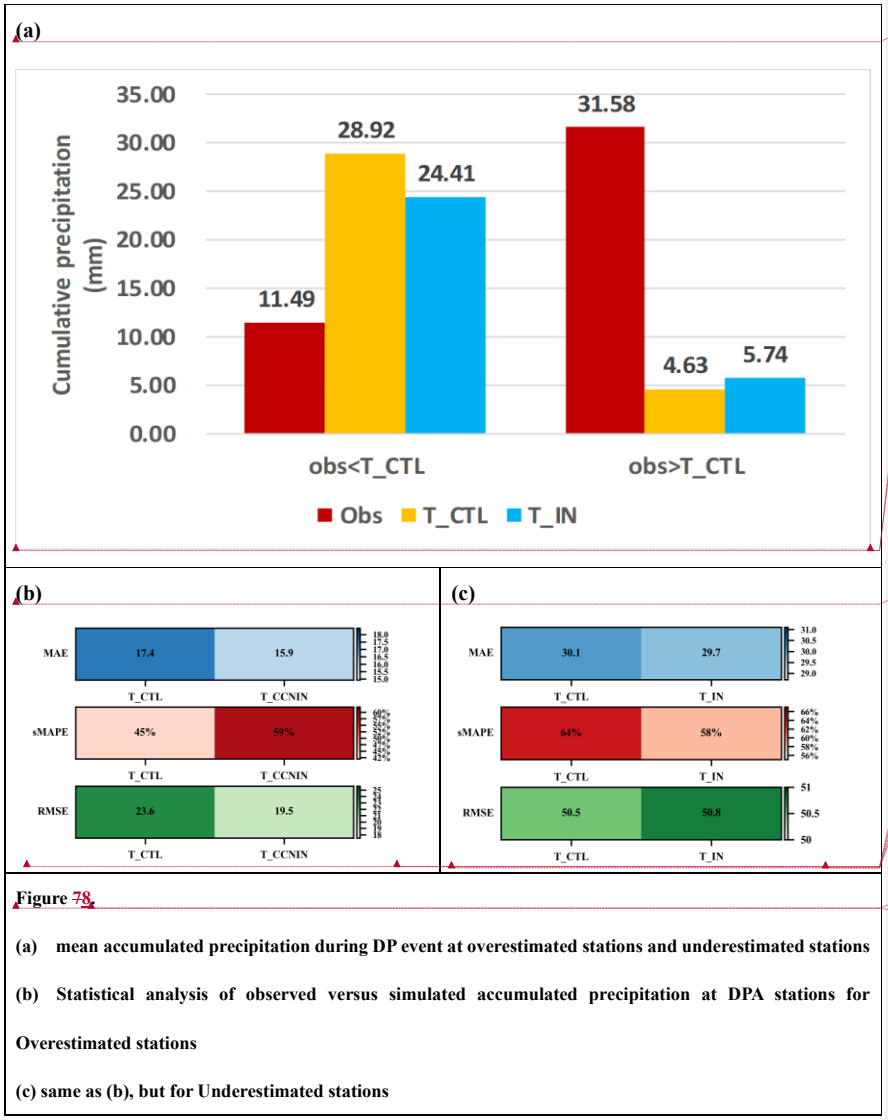


**Figure ~~7~~8.**

**(a) mean accumulated precipitation during DP event at overestimated stations and underestimated stations**

**(b) Statistical analysis of observed versus simulated accumulated precipitation at DPA stations for Overestimated stations**

**(c) same as (b), but for Underestimated stations**

带格式的: 字体: (默认) Times New Roman

带格式的: 字体: (默认) Times New Roman

带格式的: 字体: (默认) Times New Roman

带格式的: 字体: (默认) Times New Roman

带格式的: 字体: (默认) Times New Roman

带格式的: 字体: (默认) Times New Roman

带格式的: 字体: (默认) Times New Roman

带格式的: 字体: (默认) Times New Roman

带格式的: 字体: (默认) Times New Roman

带格式的: 字体: (默认) Times New Roman

## Table

**Table 1.Three Tests designed for different types of precipitation**

| Test | Warm cloud | Cold cloud |
|---|---|---|
| T_CTL | on-line aerosol–CCN interaction scheme | original WDM6 |
| T_IN | on-line aerosol–CCN interaction scheme | on-line aerosol-IN nucleation scheme |

**Table 2. List of Symbols**

| Symbol | Meaning |
|---|---|
| Paacw | Production rate for accretion of cloud water by averaged snow/graupel (Under subfreezing conditions (T < 0 °C), the collected droplets are typically supercooled and freeze onto the surface of snow or graupel particles. In this case, cloud water is converted into snow or graupel, and latent heat of fusion is released, contributing to local warming. Under above-freezing conditions (T > 0 °C), the accreted droplets do not freeze.) |
| Pcact | Production rate for cloud droplet activation from CCN |
| Pcond | Production rate for condensation rate of water vapor to cloud liquid water |
| Pgacr | Production rate for accretion of rain by graupel |
| Pgaci | Production rate for accretion of cloud ice by graupel |
| Pgaut | Production rate for aggregation form snow to graupel |
| Piacr | Production rate for accretions of rain by cloud ice |
| Pidep | Production rate for deposition- sublimation rate of cloud ice |
| Pigen | Production rate for heterogeneous nucleation |
| Pinud | Production rate for deposition/condensation freezing to form cloud ice |
| Pinui | Production rate for immersion freezing of cloud water to form cloud ice |
| Pracs | Production rate for accretions of cloud snow by rain |
| Pracw | Production rate for accretion of cloud water by rain |
| Praci | Production rate for accretion of cloud ice by rain |
| Praut | Production rate for aggregation form cloud water ice to form rain |

带格式的: 字体: (默认) Times New Roman
带格式的: 字体: (默认) Times New Roman
带格式的: 字体: (默认) Times New Roman
带格式的: 非突出显示
带格式的: 字体: (中文) 宋体, 字体颜色: 黑色
带格式的: 字体: (中文) 宋体, 字体颜色: 黑色
带格式的: 非突出显示

| | |
|---|---|
| Prevps | Production rate for evaporation/condensation rate of cloud water |
| Prevp | Production rate for evaporation/condensation rate of rain |
| Psacr | Production rate for accretions of rain by cloud snow |
| Psaci | Production rate for accretion of cloud ice by snow |
| Psaut | Production rate for aggregation form cloud ice to snow |
| Pscar | Production rate for accretion of rain by snow |
| Psdep | Production rate for deposition- sublimation rate of cloud snow |

~~Supplementary Figure 1~~

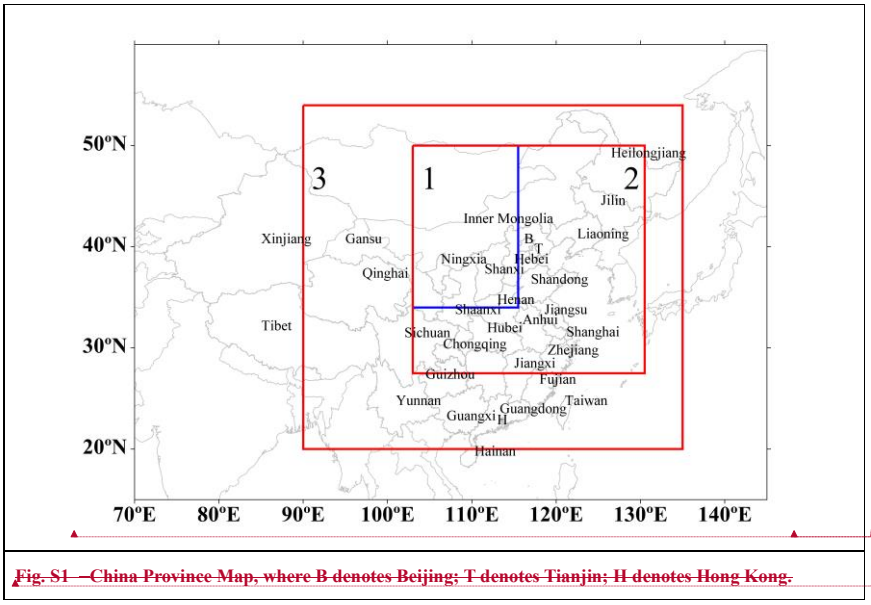


~~Fig. S1 –China Province Map, where B denotes Beijing; T denotes Tianjin; H denotes Hong Kong.~~

带格式的: 字体: (默认) Times New Roman

带格式的: 字体: (默认) Times New Roman

带格式的: 字体: (默认) Times New Roman